Ozone pollution: What can we see from space? A case study

G. Foret, M. Eremenko, J. Cuesta, P. Sellitto, J. Barré, B. Gaubert, A. Coman, G. Dufour, X. Liu, M. Joly, et al.

AGU PUBLICATIONS

JGR

Journal of Geophysical Research: Atmospheres

RESEARCH ARTICLE
10.1002/2013JD021340

Key Point:
- Ability of satellite to detect ozone pollution is evaluated

Correspondence to:
G. Foret,
foret@lisa.u-pec.fr

Citation:
Foret, G., et al. (2014), Ozone pollution: What can we see from space? A case study, *J. Geophys. Res. Atmos.*, *119*, 8476–8499, doi:10.1002/2013JD021340.

Received 11 DEC 2013
Accepted 20 MAY 2014
Accepted article online 24 MAY 2014
Published online 8 JUL 2014

Ozone pollution: What can we see from space? A case study

G. Foret[1], M. Eremenko[1], J. Cuesta[1], P. Sellitto[1,2], J. Barré[3,4], B. Gaubert[1], A. Coman[1], G. Dufour[1], X. Liu[5], M. Joly[4], C. Doche[6], and M. Beekmann[1]

[1]Laboratoire Interuniversitaire des Systèmes Atmosphériques, UMR7583, IPSL, CNRS, Université Paris Est Créteil, Université Paris Diderot, Créteil, France, [2]Laboratoire de Météorologie Dynamique, UMR8539, IPSL, CNRS, École Normale Supérieure, Paris, France, [3]ACD, NESL, National Center for Atmospheric Research, Boulder, Colorado, USA, [4]CNRM/GAME UMR 3589 CNRS/Météo-France, Toulouse, France, [5]Harvard-Smithsonian Center for Astrophysics, Cambridge, Massachusetts, USA, [6]Météo-France/DIRSO/DEC/FDF, Mérignac, France

Abstract Due to its impact on environment, tropospheric ozone received particular attention since several decades. Ground-based networks associated with regional chemical transport models are used to monitor and forecast surface ozone concentrations, but coverage, representativeness, and accuracy issues remain important. Recent satellite observations have demonstrated the capacity to probe tropospheric ozone, but there has been no explicit attempt to quantify their ability to measure ozone pollution near ground. We propose here to assess the ability of ozone sounders to detect a photochemical ozone pollution event that is supposed to be a favorable situation for satellite detection. We have chosen ozone pollution event over Europe associated with a warm conveyor belt that efficiently transports photochemically produced ozone upward. Ozone satellite products from Global Ozone Monitoring Experiment-2, Infrared Atmospheric Sounding Interferometer (IASI), and Ozone Monitoring Instrument are analyzed here for their capacity to capture such an event. Also, in situ observations and regional chemical-transport models show increasing ozone concentrations in the continental and Mediterranean boundary layer and further transport to central Europe and Scandinavia associated with upward transport. Satellite observations do not detect high ozone concentrations within the boundary layer due the weak sensitivity near the surface. Nevertheless, we have shown that the IR sounder IASI was able to detect, qualitatively and quantitatively, the ozone plume transported upward by the warm conveyor belt, suggesting that a quantification of upward transport of ozone pollution could be possible using current satellite observations. This should encourage us to further explore approaches more sensitive to surface ozone (such as the multispectral approach) and to prepare the next generation of still more sensitive spaceborne instruments.

1. Introduction

Tropospheric ozone is associated with well-known environmental issues. It is recognized as the third greenhouse gas and also as a strong oxidant involved in the budget of methane as a source of the OH radical [*Forster et al.*, 2007]. In addition, ozone near the surface is a pollutant with strong adverse effects on human health and vegetation [*Hayes et al.*, 2007; *Sitch et al.*, 2007; *World Health Organization*, 2013]. To understand, quantify, and if possible mitigate its impact on the environment, we need to be able to know its concentrations (and their evolution) from global to local scale. In Europe, background ozone concentrations are controlled on one hand by the import of ozone-rich air masses from the stratosphere into the troposphere [*Crutzen et al.*, 1999] and on the other hand by continental and intercontinental transport [*Fiore et al.*, 2009]. In the remote troposphere, ozone is chemically produced by the slow oxidation of methane and carbon monoxide [*Crutzen et al.*, 1999], in the presence of nitrogen oxide (NO) and UV radiation. In the polluted planetary boundary layer (PBL), the same processes occur at larger speed due to the oxidation of short-lived volatile organic compounds (VOCs).

This photochemical ozone production takes place over the most populated continental areas where strongest emissions of ozone precursors occur. Finally, the balance is ensured by the dry deposition of ozone over solid surfaces (especially vegetation). Surface measurement networks over populated areas and at some remote locations enable an accurate (but spatially incomplete) monitoring of surface ozone concentrations. These networks are complemented by vertical soundings and measurements made on board of commercial aircraft [*Marenco et al.*, 1998] and balloons that allow, for example, a better view of long-range transport.

Regional chemical transport models (rCTMs) are efficient monitoring tools for ozone concentrations providing also forecasting capabilities. Based on such tools, operational platforms exist now in several European countries (see *Kukkonen et al.* [2012] for a review). The goals of these platforms are manifold ranging from operational forecasting of severe ozone episodes to verification of long-term exposure and mitigation scenarios. As a consequence, to improve the accuracy and operational aspects of such tools is now mandatory. This is the purpose of several international programs (Seventh Framework Programme/Monitoring Atmospheric Composition and Climate-Interim Implementation (MACC-II) (http://www.gmes-atmosphere.eu/) and Air Quality Model Evaluation International Initiative [*Rao et al.*, 2011]). Following approaches used in meteorology and oceanography, the monitoring and forecasting tools developed for air quality are now using in a synergistic manner model and observations based on assimilation techniques [*Elbern and Schmidt*, 2001; *Blond and Vautard*, 2004; *Hanea et al.*, 2004; *Wu et al.*, 2008].

In this context, the use of satellite observations for pollution monitoring and evaluation is becoming more and more popular. For the case of ozone, the last generation of spaceborne sounders is offering increased opportunities to observe tropospheric ozone, either using UV/VIS (ultraviolet/visible) instruments like Global Ozone Monitoring Experiment-2 (GOME-2) [see *European Organisation for the Exploitation of Meteorological Satellites*, 2006] or Ozone Monitoring Instrument (OMI) [*Levelt et al.*, 2006] or using TIR (thermal infrared) instruments like Tropospheric Emission Spectrometer (TES) [*Worden et al.*, 2007] or Infrared Atmospheric Sounding Interferometer (IASI) [*Clerbaux et al.*, 2009]. Concerning UV instruments, *Liu et al.* [2010] have shown, for the case of the OMI, the potential of this sounder to detect and follow tropospheric ozone plumes. Nevertheless, direct vertical sensitivity to boundary layer concentrations is rarely achieved due to reduced sensitivity to lower tropospheric ozone and coarse vertical resolution. *Kar et al.* [2010] demonstrated the capability of these UV/VIS instruments to occasionally "see" urban plume signatures but at monthly temporal scales and more efficiently for isolated urban centers. Also, *Wang et al.* [2011] shows a good agreement between sondes and OMI in the middle troposphere but large discrepancies between OMI and surface observations in the case of high ozone concentrations. On the other hand, several studies have already shown the potential of TIR instruments to monitor ozone concentrations in the troposphere and also in the lower troposphere. In the case of IASI observations, the accuracy of the surface to 6 km partial columns has been demonstrated with errors generally lower than 20% at midlatitudes [*Keim et al.*, 2009; *Dufour et al.*, 2012]. TES observations have already been used to analyze particular ozone features such as the Eastern Mediterranean and Middle East maxima during summer in the free troposphere [*Liu et al.*, 2009; *Worden et al.*, 2009; *Richards et al.*, 2013]. This is also the case of IASI observations that have been used to investigate ozone pollution over polluted regions like China [*Dufour et al.*, 2010] or Europe [*Zyryanov et al.*, 2012]. Due to its twice daily coverage and a large across-track swath, IASI has proven to be capable of qualitatively probing events of elevated tropospheric ozone concentrations at daily scale, i.e., a photochemical pollution event over eastern Europe [*Eremenko et al.*, 2008], a deep stratospheric intrusion over Europe [*Zyryanov et al.*, 2012], the predominance of stratospheric intrusions that explain large ozone observed over Beijing region in winter than in spring and summer, enhanced partial columns of ozone are observed in coincidence with pollution alerts [*Dufour et al.*, 2010]. This ability is, of course, of primary importance in the context of air quality. Moreover, these observations can be used to correct models. *Parrington et al.* [2008] have shown how the assimilation of TES observations could improve the representation of modeled-free tropospheric concentrations over a summer period. On the other hand, *Parrington et al.* [2009] show that if the assimilation of TES observations was modifying surface modeled fields, this did not result in a general model improvement. More recently, using not only TES but also OMI ozone observations, *Huang et al.* [2013] investigated the ability of these observations to detect a long-range transport episode and to further correct (via assimilation) the representation of boundary layer ozone in a CTM. They conclude that these observations were not very efficient in correcting the model in this case because of a lack of spatial coverage and maybe inadequate accuracy of these satellite data observations. Similarly, *Coman et al.* [2012] have assimilated IASI surface to 6 km ozone partial columns, allowing to reduce the model bias not only in the free troposphere but also at the surface. Improvement at the surface was partially due to downward transport of free tropospheric air masses, where the fields are preferentially corrected by IASI observations. Such situations occur when persistent subsiding anticyclonic conditions are present [*Foret et al.*, 2009].

In spite of these numerous applications, the capability of satellite ozone observations to detect photochemical pollution occurring events within the boundary layer has not been clearly and definitively demonstrated and

quantified. In the case of UV instruments, it has been demonstrated that while OMI has a significant sensitivity to the tropospheric ozone column, it has small sensitivity to lower tropospheric ozone [*Sellitto et al.*, 2011]. In fact, the sensitivity of OMI retrievals to the boundary layer is not fully exploited, due to interference with aerosols and surface albedo [*Liu et al.*, 2010]. Nevertheless, in the case of low cloud cover the sensitivity can be significantly improved in the lower part of the troposphere above clouds [*Liu et al.*, 2010]. In the case of TIR measurements, observations are generally not very sensitive to surface ozone concentrations. Nevertheless, pollution events, which are one of the main targets of air quality monitoring and forecasting, present some peculiarities that are favorable to their detection by TIR sounders. Associated with intense photochemistry and air mass stagnation, anticyclonic situations favor the occurrence of strong ozone concentrations within the planetary boundary layer and possibly above. In such cases, cloud cover is weak and the number of available pixel (and correspondingly the amount of information) is significant. Moreover, large boundary layer heights favor mixing of surface ozone to altitudes where it can be detected. Also, a strong thermal contrast between the ground and the first atmospheric layer allows improving significantly the sensitivity of TIR instruments in lower layers. The objective of this work is to evaluate the capability of satellite instrument to observe surface and lower tropospheric ozone concentrations in the case of a high ozone event and the way through which it can be transported upward. To do so, a photochemical pollution case of moderate intensity, i.e., representative of current European pollution, associated with a warm conveyor belt has been chosen. In this case, ozone concentrations in the boundary layer are relatively high and are further lifted into the lower free troposphere by a warm conveyor belt associated with a classical frontal situation. Such conditions are recognized to be important processes to ventilate boundary layer pollution into the free troposphere at midlatitudes [*Sinclair et al.*, 2008]. In situ ozone measurements (surface and profiles) and meteorological analysis are used to characterize this event. Available satellite observations are then confronted to these observations and simulations made with rCTM. More precisely, in this study we have used ozone retrievals from GOME-2, OMI, and IASI instruments. In this case of a few days event, the use of TES retrievals was not appropriate due to the very weak sampling of the instrument.

In the following, we first give a short review of satellite products available (section 2); then we make a quick description of modeling systems (section 3). In section 4, we describe the case study from the meteorological point of view (section 4.1) and from the "ozone" point of view (section 4.2). In section 5, we discuss the capability of available satellite products to observe this pollution event. Finally, conclusions and perspectives are given (section 6).

2. Characteristics of Available Satellite Instruments and Products

Several spaceborne instruments have already evidenced their capability to observe tropospheric ozone with reasonable accuracy. However, it is still unclear if such observations can be used to observe either qualitatively or quantitatively photochemical pollution events. We present here the different instruments that could be used for such a purpose.

2.1. GOME-2 (Global Ozone Monitoring Experiment-2)

Based onboard the MetOp satellites, GOME-2 is a nadir-viewing UV/VIS spectrometer which measures daytime earth reflectance (i.e., the ratio between backscattered radiance and solar irradiance) with ground pixels of 40 km × 80 km over a swath of about 2200 km (similar to IASI). The spectral resolution is ~ 0.24 nm after convolution by the instrument response function and the sampling interval ~ 0.12 nm. The ozone retrieval scheme used in the present paper is described and validated by *Cuesta et al.* [2013]. It is originally based on the work of *Cai et al.* [2012] for forward model calculations, but with spatial resolution refined by a factor of 8 (40 km × 80 km here). The scheme implements a Tikhonov-Phillips-type regularization, for which constraints are set in a way that they match approximately the retrieval noise for the IASI approach described below. This UV ozone retrieval considers two microwindows between 290 and 345 nm accounting for the Hartley and Huggins bands (from, respectively, channels 1 and 2 of GOME-2). Measurements below 290 nm are not used because of their sensitivity essentially to stratospheric ozone and due to low signal-to-noise ratios.

2.2. IASI (Infrared Atmospheric Sounding Interferometer)

The IASI instruments [*Clerbaux et al.*, 2009] are nadir-viewing Fourier-transform spectrometers designed for operation on the meteorological MetOp satellites launched by European Organisation for the Exploitation of

Meteorological Satellites (EUMETSAT) and European Spatial Agency. The first instrument, considered in this study, was launched onboard the satellite MetOp-A on 19 October 2006 and started operational measurements in June 2007. In addition to meteorological products (surface temperature and humidity profiles, and cloud information), the large spectral coverage (645–2760 cm^{-1}), the high radiometric sensitivity and accuracy, and the rather high spectral resolution (the apodized spectral resolution is 0.5 cm^{-1}) of the instrument allow deriving global distributions of several important atmospheric trace gases among which are ozone [e.g., *Boynard et al.*, 2009], CO [e.g., *George et al.*, 2009], and ammoniac [*Clarisse et al.*, 2009]. The nadir field of view for one IASI pixel has the diameter of 12 km at the surface. The maximum scan angle of 48.3° from nadir corresponds to coverage of about 2200 km across track for one swath as for GOME-2. The retrieval of ozone profiles from IASI spectra used in the present study is based on the method described and validated in *Eremenko et al.* [2008] and *Dufour et al.* [2012].

2.3. OMI (Ozone Monitoring Instrument)

OMI is a Dutch/Finnish UV/VIS nadir-viewing push-broom spectrometer, which is embarked on the NASA-Aura spacecraft [*Levelt et al.*, 2006]. It is in the heritage of European Space Agency Global Ozone Monitoring Instrument (GOME) [*Burrows et al.*, 1999] and the Scanning Imaging Absorption Spectrometer for Atmospheric Chartography [*Bovensmann et al.*, 1999] instruments. OMI operates in the spectral interval 270–500 nm, with a spectral resolution of 0.42–0.63 nm and a direct nadir spatial resolution of 13 km along the track × 24 km across the track, in the so-called "Global Mode," while it can reach the spatial resolution of 13 km × 12 km in its "Zoom Mode." The spatial resolution at the borders of the swath is substantially lower than the nominal nadir resolution. The telescope of the OMI instrument has a wide field of view (114°), which corresponds to a 2600 km wide swath on the surface and global coverage time of 1 day. Since May 2007, a major degradation in the performances of OMI has emerged as the so-called "row anomaly," caused by a problem in the OMI nadir port, that affects OMI radiance spectra measured for particular viewing directions of the instrument. The row anomaly initially only affected a few cross-track pixels but has become more serious since January 2009, affecting more than 1/3 of the cross-track pixels. More info can be found at http://www.knmi.nl/omi/research/product/rowanomaly-background.php. The tropospheric ozone columns analyzed in the present work are derived from the ozone profile product by *Liu et al.* [2010] with several major modifications described in *Kim et al.* [2013]. To speed up processing, the retrieval is done here at a nadir resolution of 52 km × 48 km by averaging (co-adding) 4/8 OMI UV1 (270–310 nm)/UV2 (310–330 nm) pixels. A major change to the retrieval presented by *Liu et al.* [2010] is the constraint on measurement error. Recent downward revision of the OMI measurement error (smaller by a factor of 1.4–2.3) [*Braak*, 2010], together with further reduction of this error through co-adding, results in unrealistically small observational error specification (0.035% at 320 nm under tropical clear conditions) that causes spurious variability in the retrieval. Therefore, a minimum measurement error of 0.2% in the spectral region of 300–330 nm is imposed. Although this error specification stabilizes the retrievals, it significantly reduces the retrieval sensitivity compared to that in *Liu et al.* [2010]. Pixels with effective cloud fraction greater than 0.3 are considered as "cloudy" and are screened out. The remaining pixels are quality checked by means of the quality flags in the Level 2 data, and pixels affected by the row anomaly are further excluded from the analysis.

3. Description of the Modeling System

For this study, we used two state-of-the-art rCTMs, CHIMERE [*Menut et al.*, 2013] and MOCAGE [*Barré et al.*, 2013]. Configurations of both models are derived from the operational versions that have been set up for the MACC-II project [*Barré et al.*, 2012; *Zyryanov et al.*, 2012]. The geographical domain covered is roughly western Europe as shown in Figure 1. The horizontal resolution is 0.2° × 0.2° for MOCAGE and 0.25° × 0.25° for CHIMERE. MOCAGE covers a vertical domain from the surface to the upper stratosphere (5 hPa) using 23 hybrid (σ, p) vertical levels within the troposphere. CHIMERE covers the troposphere (from the surface to 200 hPa) with a similar vertical discretization (20 hybrid (σ, p) levels). Different parameterizations used in both models are summarized in Table 1. For advection, the MOCAGE model uses a semi-Lagrangian approach [*Williamson and Rash*, 1989], while CHIMERE uses a sixth-order [*Colella and Woodward*, 1984] or third-order [*Van Leer*, 1979] scheme in an Eulerian framework. Chemical modules are also different, since in the MOCAGE model, tropospheric and stratospheric chemistry of ozone are represented, which is not the case in the CHIMERE model with only tropospheric chemistry. Dry deposition schemes both follow the "resistance" approach [*Wesely*, 1989].

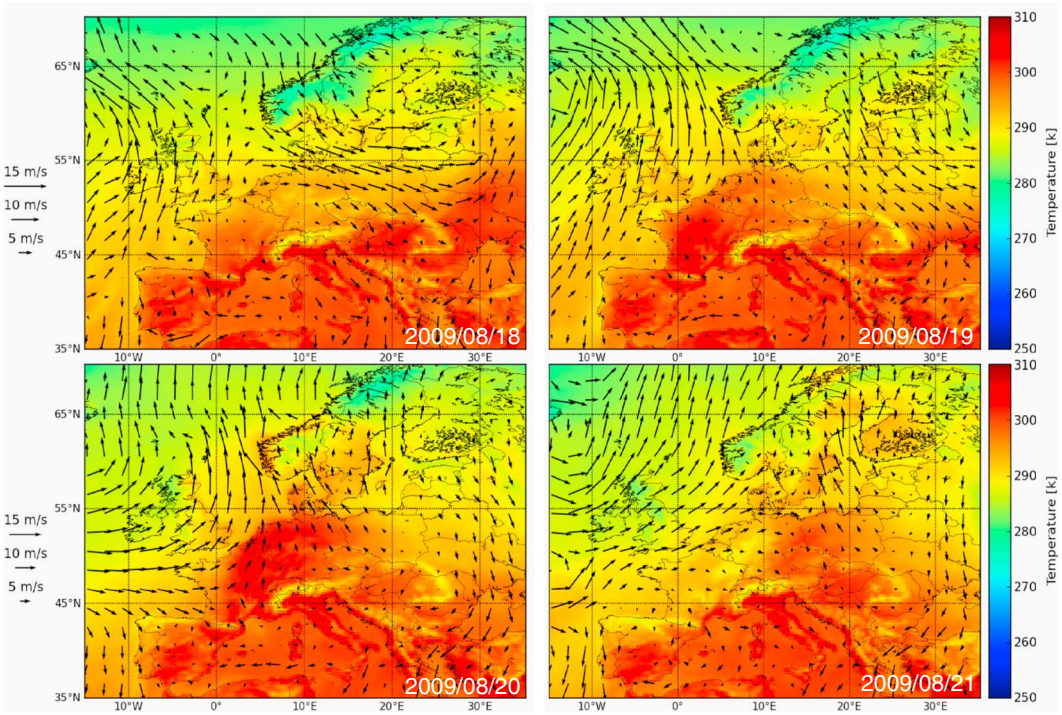

Figure 1. Two-meter temperature fields and surface winds from IFS at 3 P.M. for (top left) 18 August 2009, (top right) 19 August 2009, (bottom left) 20 August 2009, and (bottom right) 21 August 2009.

Among external forcings, only anthropogenic emission inventories are similar for both models (TNO inventory) [*Visschedijk et al.*, 2007]. Other model forcings are different: MOCAGE is using the meteorological analysis from ARPEGE [*Courtier et al.*, 1991] at a 3 h frequency, and chemical boundary conditions are provided by the MOCAGE-CTM itself; for both meteorology and the boundary conditions, CHIMERE is using European Centre for Medium-Range Weather Forecast (ECMWF) products, i.e., 3-hourly forecast of Integrated Forecasting System (IFS) and Model for Ozone And Related chemical Tracers (MOZART)-IFS. In conclusion, both rCTMs are significantly different in their formulation and their input data, and their simultaneous use will give robustness to the analysis and comparisons performed in this work.

4. Description of the Case Study

For this study, we have chosen an ozone pollution event of moderate intensity. It is characterized by high surface ozone concentrations sometimes exceeding 90 ppb (i.e., the information threshold of ozone in Europe). It is one of the most important events during summer 2009 [*European Environmental Agency*, 2010], but if compared to ozone pollution events occurring between 2007 to 2012, we consider it as a rather typical event for western and central Europe [*European Environmental Agency*, 2013a] far from high pollution events occurring in 2003 and 2006 [*European Environmental Agency*, 2013b]. It occurred in August 2009 (19–21). Moreover, during this period, air masses are lifted from the boundary layer upward due to the presence of a warm conveyor belt transferring polluted air masses into the lower free troposphere as it is frequently observed at northern midlatitudes in the vicinity of frontal systems.

Table 1. Main Parameterizations Used for CHIMERE and MOCAGE Models

	Natural Emissions	Chemistry	Advection	Convection	Diffusion	Dry Deposition
CHIMERE [*Menut et al.*, 2013]	*Guenther et al.* [2006]	MELCHIORII; *Schmidt et al.* [2001]	*Colella and Woodward* [1984]; *Van Leer* [1979]	*Tiedtke* [1989]	*Troen and Mahrt* [1986]	*Zhang et al.* [2003]
MOCAGE [*Josse et al.*, 2004; *Bousserez et al.*, 2007]	*Guenther et al.* [1995]; *Dentener et al.* [2005]	RACM; *Stockwell et al.* [1997]; + REPROBUS; *Lefèvre et al.* [1994]	Semi-Lagrangian [*Williamson and Rash*, 1989]	*Bechtold et al.* [2001]	*Louis* [1979]	*Michou and Peuch* [2002]

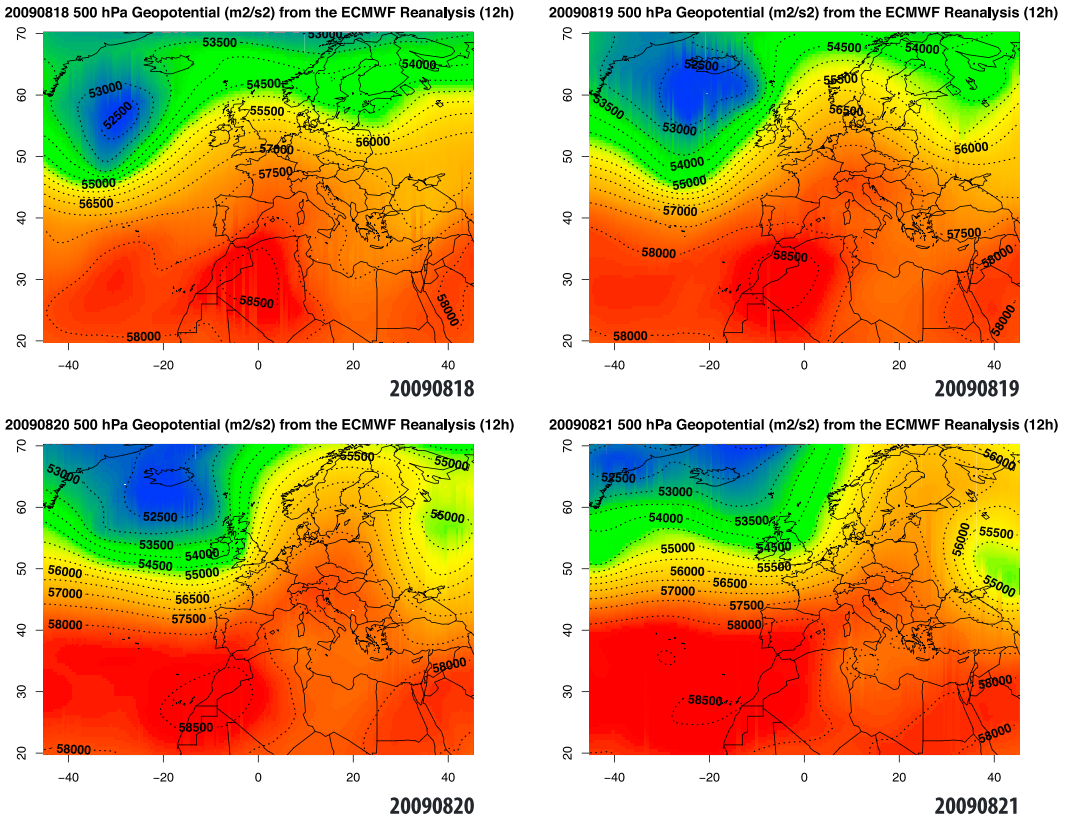

Figure 2. Geopotential height fields at 500 hPa from IFS at noon for (top left) 18 August 2009, (top right) 19 August 2009, (bottom left) 20 August 2009, and (bottom right) 21 August 2009.

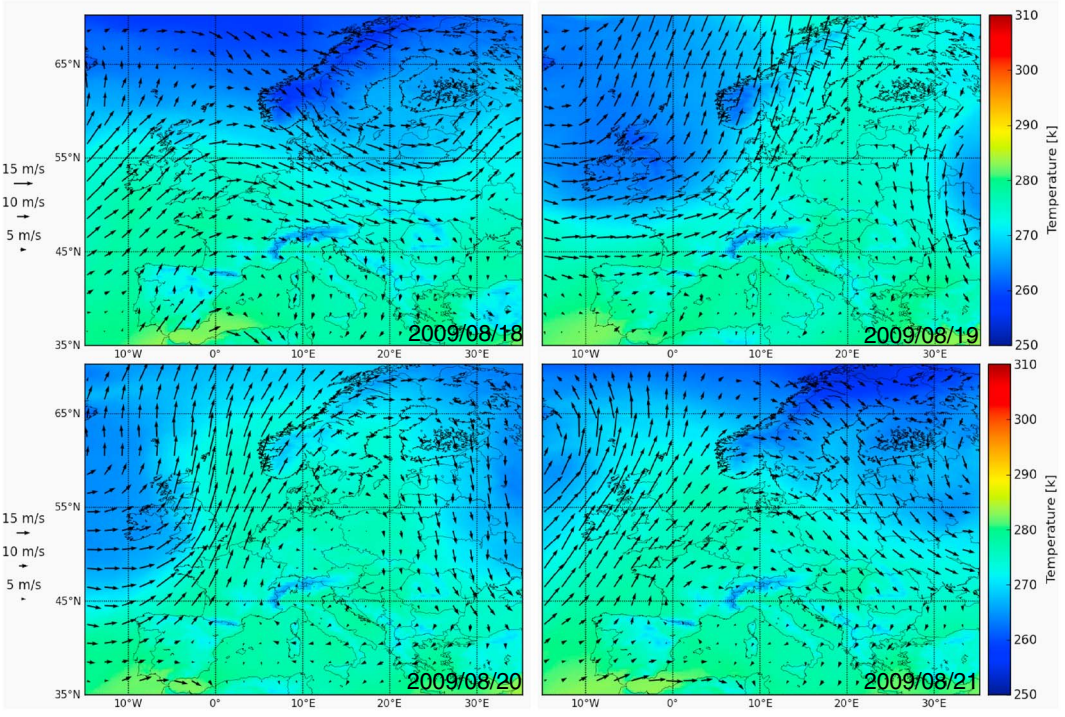

Figure 3. Three-kilometer height temperature and wind fields from IFS at 3 P.M. for (top left) 18 August 2009, (top right) 19 August 2009, (bottom left) 20 August 2009, and (bottom right) 21 August 2009.

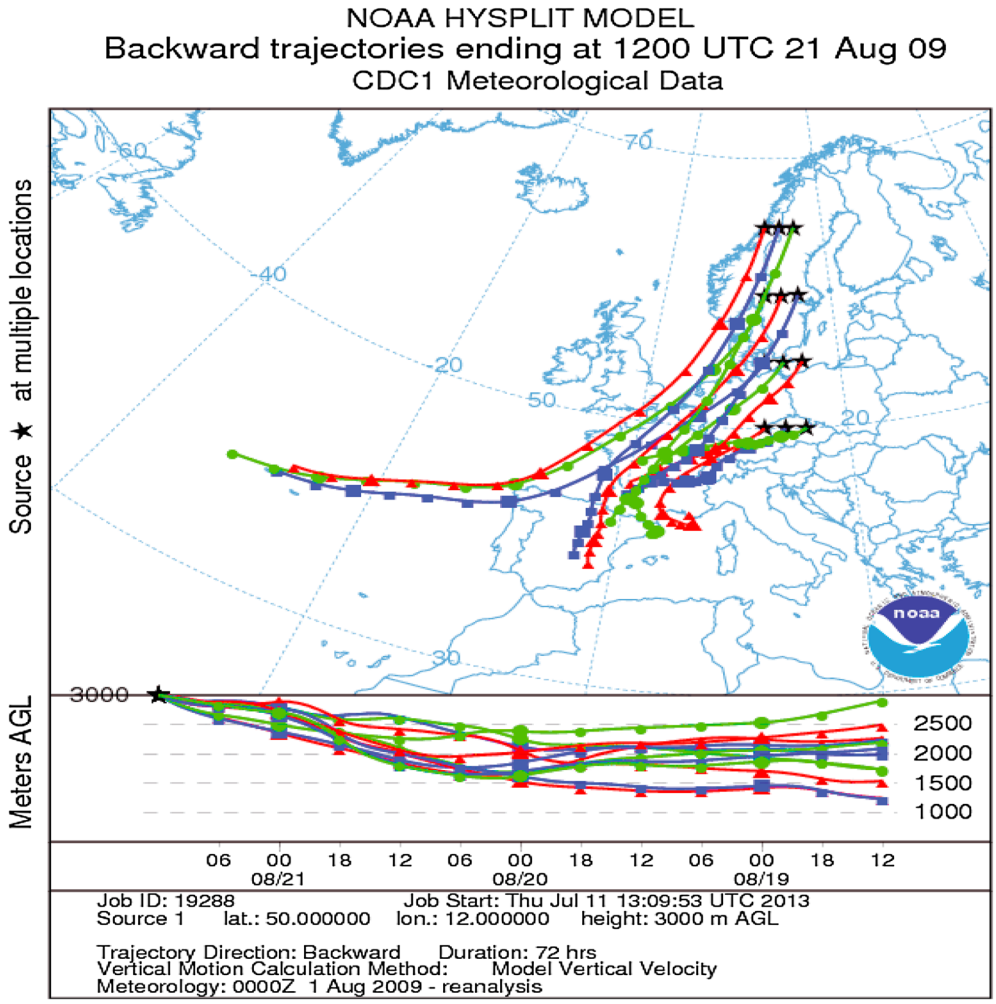

Figure 4. HYSPLIT (Hybrid Single Particle Lagrangian Integrated Trajectory) backtrajectories calculated for all points of the grid (black stars). Trajectories are calculated backward from 21 August 2009 at noon at (left) 3 km altitude and at (right) 1.5km altitude for 72 h (http://www.ready.noaa.gov).

4.1. Meteorological Situation

To describe the meteorological situation, we use analysis (every 12 h) and forecast (3-hourly between analyses) from the Integrated Forecasting System (IFS) of the European Centre for Medium-Range Weather Forecast (ECMWF). On 19 August 2009, an anticyclonic situation set up over western Europe and especially over France; it was characterized by low wind speed (and associated weak dispersion), high surface temperatures above 30°C (Figure 1), generally a good proxy of ozone pollution, and low cloud cover. The next day (20 August 2009), a low-pressure system arrived at the western tip of France. On 21 August 2009, this structure propagated eastward with still high temperature on its eastern side. Also, geopotential height at 500 hPa confirms this evolution, with the presence of an anticyclonic situation over Europe followed by a more and more baroclinic circulation with the formation of a through over western Europe and a ridge over central Europe (Figure 2). A frontal structure extending from southwest to northeast along geopotentiel isolines is observed (Figure 2), presenting strong temperature gradients at 3 km altitude (Figure 3). It is linked to a warm conveyor belt ahead of the low-pressure system associated with a cloud band along the front (not shown).

Warm conveyor belts favor the transport of air masses from the boundary layer to the free troposphere. They are characterized by warm air streams that are uplifted along and ahead a cold front [*Bethan et al.*, 1998; *Kowol-Santen et al.*, 2001; *Agustí-Panareda et al.*, 2005, 2009]. HYSPLIT back trajectories [*Rolph*, 2013] show that air masses arriving at 3 km altitude are mainly uplifted from layers below (1000 to 2000 m altitude) along the frontal area (Figure 4, left). The same behavior is observed for air masses arriving at 1.5 km altitude that are uplifted

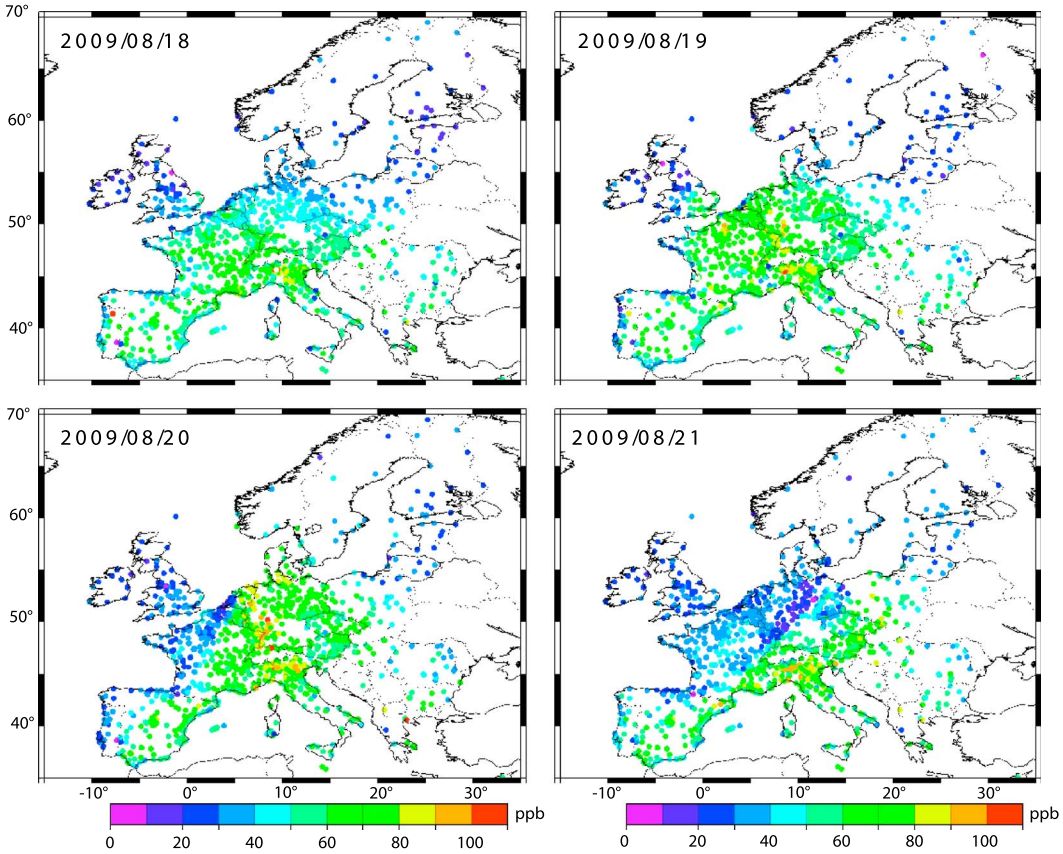

Figure 5. Surface ozone concentrations (ppb) at 3 P.M. at European (background urban, suburban, and rural) stations (http://acm.eionet.europa.eu/databases/airbase/).

mainly from 500 to 1000 m height. The horizontal component of trajectories follows geopotential isolines with a southwest to northeast orientation. The vertical component shows an upward transport of continental air masses from France and Spain (Figure 4, most of green and blue trajectories) and also from the Mediterranean area (Figure 4, red trajectories). Moreover, PV (Potentiel vorticity) field from ECMWF have been inspected and have shown low PV values in the area of the ozone plume, confirming no stratospheric influence during this event.

4.2. Tropospheric Ozone Fields

Associated with this meteorological situation, ozone concentrations and their space-time evolution are now investigated using in situ measurements. rCTMs are also used to analyze the four-dimensional evolution of ozone fields and to understand the driving forces of their variability.

4.2.1. In Situ Observations

Ground-based ozone measurements made by regional and national networks are gathered and made available through the Airbase database (http://acm.eionet.europa.eu/databases/airbase/). For summer 2009, we dispose of hourly ozone concentrations at about 1200 stations. From those, we select 694 mostly background stations in an urban, suburban, or rural environment, i.e., industrial and traffic stations are removed because of their too local spatial representativeness. The afternoon ozone concentrations (~3 P.M.) show the formation of the pollution event on 19 August 2009 especially over France (Figure 5). Associated with the passage of the eastward moving front, sharp gradients in ozone concentrations are observed on 20 and 21 August, with clean air masses over western Europe (30–40 ppb) while stronger ozone concentrations (>60 ppb) appear eastward of the frontal area.

During this 3 day period, hourly ozone concentrations exceeding 90 ppb (i.e., the information threshold at which population has to be informed about high ozone levels) have been observed more than 300 times mostly over France, Germany, and Italy (Figure 5). Only one station in France has measured ozone concentrations above

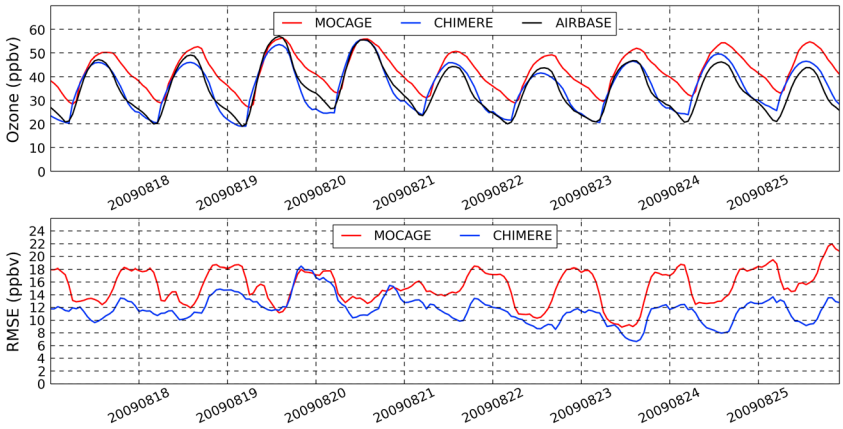

Figure 6. (top) Ozone time series (between 17 and 25 August 2009) in ppb averaged over all surface stations shown in Figure 5 (black curve) and simulated by CHIMERE (blue curve) and MOCAGE (red curve) and (bottom) corresponding root-mean-square errors.

120 ppb (alert threshold) on 19 August 2009. Also on the average over all sites, largest ozone values appear on 19 and 20 August, around noon (Figure 6). This situation with enhanced ozone levels and well-defined gradients is a good opportunity to evaluate the capability of spaceborne sensors to detect surface ozone concentrations.

In addition, ozone vertical profiles measured onboard commercial aircrafts taking off and landing at Frankfurt (Measurement of Ozone on Airbus In-service airCraft (MOZAIC) program) clearly show the increase of ozone concentrations on 19 and 20 August (about 70 ppb at 800 m above surface layer) corresponding to the pollution event and the decrease of concentrations on 21 August after the passage of the frontal area (Figure 7).

Back trajectories from the NOAA HYSPLIT model (http://ready.arl.noaa.gov/HYSPLIT.php) have been used to analyze vertical profiles from MOZAIC. For the 1 km altitude peak on 19 and 20 August, trajectories show that air masses originate from a similar altitude and have had continental pathways for at least 2 days prior to the measurements (Figure A1). Thus, they had the opportunity to accumulate ozone precursor emissions within the boundary layer (which height exceeded 1 km during afternoon over continental areas). This led to progressively increasing ozone levels. Above, at 2 km altitude, for example, we see that air masses arriving around Frankfurt on 19 August have mostly experienced zonal trajectories from the west as well as downward motion from above 3 km height and thus were probably not affected by surface emissions over Europe, corresponding to much lower background ozone concentrations. On the contrary, trajectories arriving on 20 August have more continental yet subsiding trajectories from the southwestern quadrant with possible mixing with boundary layer air masses especially over Spanish plateau where the PBL height can reach several kilometres (Figure A2). These differences can explain the higher concentrations observed on 20 August above 1 km altitude.

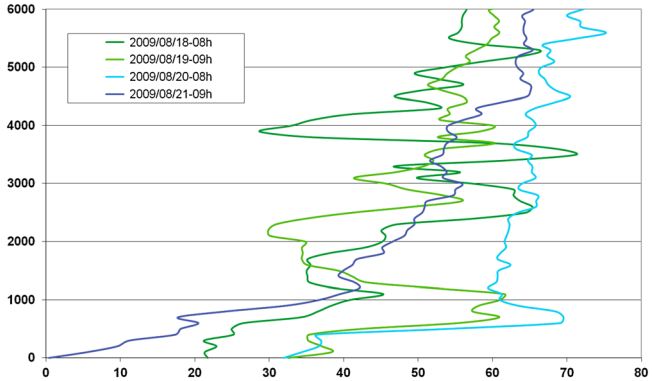

Figure 7. Ozone vertical profiles (ppb) around Frankfurt airport measured in the MOZAIC/IAGOS (In-service Aircraft for a Global Observing System) framework between 18 and 21 August 2009.

As a conclusion, there is a clear buildup of surface ozone concentrations between 18 and 20 August 2009. The occurrence of a cyclonic circulation from the west swept off polluted air masses to the northeast. Meteorological analysis and trajectory calculations suggest the presence of a warm conveyor belt related to the frontal system which allows for uplifting of boundary layer air masses with large ozone concentrations to higher altitudes. In the next section, we use rCTMs to investigate and analyze these features in more detail.

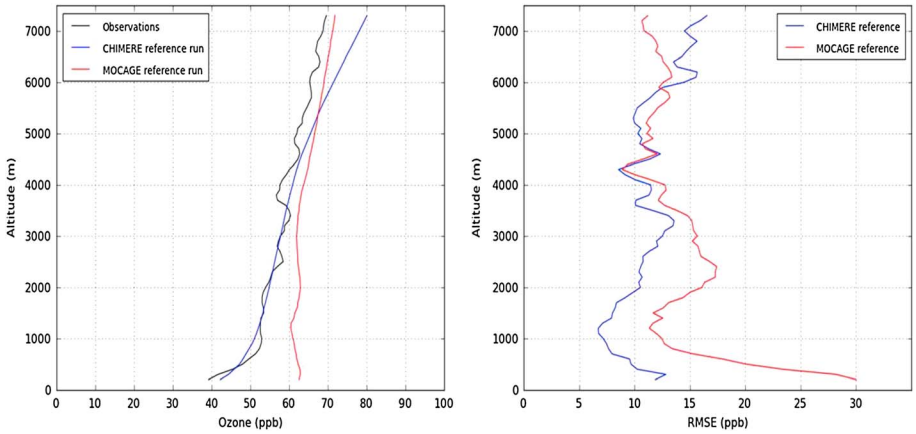

Figure 8. (left) Ozone mean vertical profiles (ppb) for available ozonesondes and MOZAIC flights. Observations are in black, CHIMERE simulation in blue, and MOCAGE simulation in red. (right) Corresponding errors (RMSE). Mean values are calculated over 100 m thick layers for 11 sondes (data from WOUDC (http://www.woudc.org) and NADIR (http://www.nilu.no/nadir/)) and 17 MOZAIC flights at Frankfurt.

4.2.2. Analysis of the Event Using Model Simulations

We use rCTMs to complement the analysis of the pollution event and in particular to explore the processes driving ozone concentration variations. Several studies have shown that these models are now accurate enough to constitute an independent and reliable source of information to study ozone pollution events especially over Europe [*Solazzo et al.*, 2012; *Zyryanov et al.*, 2012]. The strength of the model is to provide a full four-dimensional view of the event. In order to be confident that models behave well to simulate our case study, we have first evaluated their accuracy against available surface measurements and ozone vertical profiles from sondes and aircraft. Results are very similar to those of previous studies over longer time periods [*Jaumouillé et al.*, 2012; *Zyryanov et al.*, 2012]. Figure 6 shows that models well reproduce the mean ozone diurnal cycle at the surface with a positive bias for MOCAGE and a slightly negative bias for CHIMERE (most pronounced for 21 August 2009) during daytime. A larger overestimation of MOCAGE ozone simulations is also observed mostly during nighttime (generally above 10 ppb at midnight). This feature, also observed to a lesser extent for CHIMERE, is often due to the difficulty of models to well reproduce low boundary layer heights and associated more efficient ozone losses by dry deposition and by titration with NO [*Gaubert et al.*, 2014]. *Gaubert et al.* [2014] also point out that in such conditions the representativeness of ground-based stations is often reduced, inducing specific nighttime biases when compared to the ozone concentrations in the first model layer. In general, RMSEs (root-mean-square errors; Figure 6, bottom) are in the range 8 to 18 ppb with mean values of about 12 ppb for both models during daytime. Up to 7 km, both models exhibit almost constant RMSE with values in the range of 8 to 15 ppb except for large MOCAGE RMSE of 15–30 ppb near the surface (Figure 8). It should be noted that over such a short time period, only 28 profiles are available over the European domain, leading to less robust results than those presented for the surface.

The inspection of both simulated ozone fields at the surface (and at 10 A.M.) confirms the setup of the pollution event on the 19 August 2009 over western Europe and the following propagation of the pollution plume eastward and northward on the eastern side of the cyclonic circulation along the frontal pattern (Figure 9). From this figure, we also can see that the ozone-rich structure observed at the surface is still present in altitude, i.e., at 3 km and to a lesser extent at 5 km. It broadly follows the contours of the high-pressure ridge at 500 hPa present over central Europe (Figure 2). Along its western edge, a northeasterly flow advects ozone-rich air masses from the Spanish plateau and from the Mediterranean area toward Scandinavia (Figure 3). As shown below, additional ozone transport occurs by vertical uplifting of air masses.

To quantify and understand more precisely the contribution of photochemically formed ozone in the European boundary layer to tropospheric ozone fields, we carried out a sensitivity model analysis using the rCTM CHIMERE. We have calculated simulated surface to 6 km partial columns for simulations in which surface emissions (anthropogenic and natural) have been switched off. Several experiments have been conducted by cutting off emissions from 19, 18, 17, and 16 August on and without any emissions for the whole August simulation. For 20 August 2009, the simulation without any emissions during August (i.e., ozone concentrations

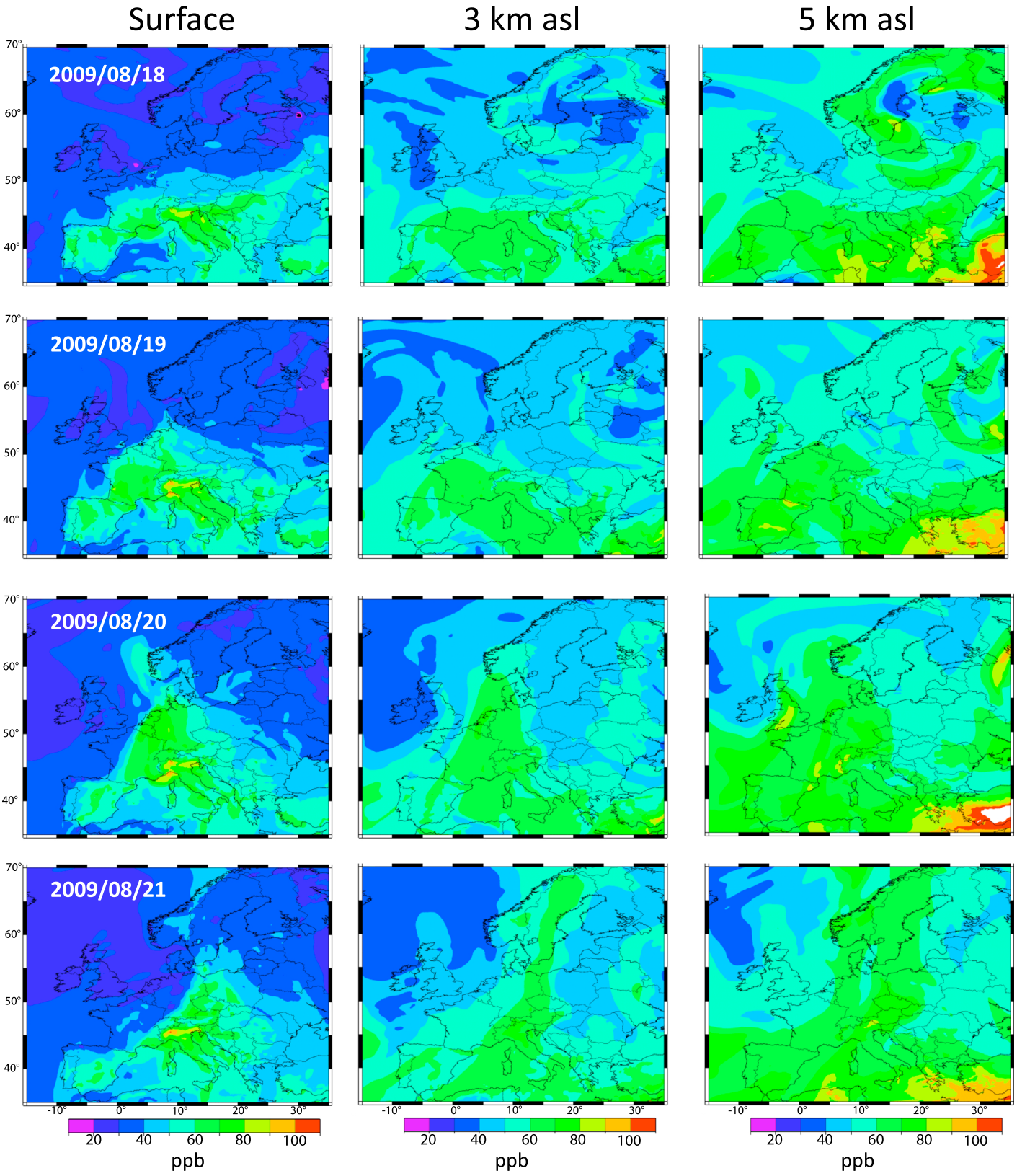

Figure 9. CHIMERE-simulated ozone concentrations (ppb) at 10 A.M. and at three different altitudes above surface layer (surface, 3 km, and 5 km) for the period ranging from 18 to 21 August 2009.

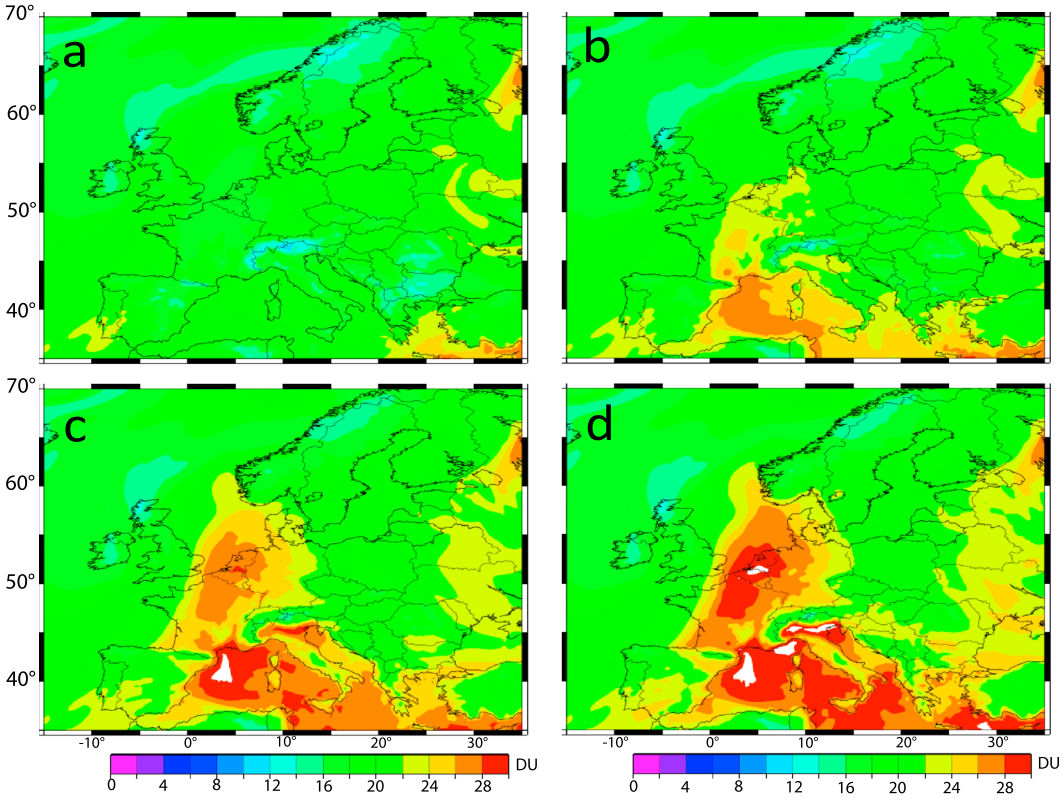

Figure 10. Simulated ozone columns (surface to 6 km in DU) for 20 August 2009 (10 A.M.) when emissions are switched off (a) since 1 August 2009; (b) since 17 August 2009; (c) since 19 August 2009; and (d) when emissions are present.

are mainly controlled by the transport of boundary conditions into the domain) shows rather homogeneous column values ranging from 20 to 22 Dobson unit (DU) (Figure 10a). On the contrary, the control run (i.e., with full emissions) shows (Figure 10d) much higher values (up to 30 DU) on the Mediterranean basin and in the plume along the frontal area, indicating that these air masses contain photochemically produced ozone. Intermediate values for column ozone are obtained if emissions are cut later (Figures 10b and 10c). These sensitivity simulations indicate that large ozone levels near ground and in the free troposphere are controlled not only by the precursor emissions from the previous day but also by the emissions of at least 3 days before. Figure 9 shows that enhanced ozone partial columns are due to enhanced ozone concentrations not only in the boundary layer but also in the free troposphere. As the spatially homogeneous ozone fields in Figure 10a exclude horizontal advection of ozone-rich air masses, this suggests that during this episode, photochemically produced ozone accumulated in the boundary layer and/or precursors (NO_x, VOC) allowing further ozone production are subsequently lifted. Figures 10b and 10c show that even when switching off emissions during the pollution episode, this transport occurs. They suggest transport of ozone-rich air masses from the Mediterranean area to higher latitudes, following the SW-NE-directed flow induced by the ridge system. Trajectory calculations (Figure 4) and the wind patterns (Figures 1 and 3) confirm this transport and also show its ascending nature.

To further determine the quality of the observations of each instrument, we have also plotted the surface to 6 km ozone (raw) columns as seen by the rCTMs CHIMERE and MOCAGE. The results (Figure 11) show quite consistent modeled ozone fields in terms of the structure of the pollution event and of the amount of simulated ozone. The positive bias of MOCAGE compared to CHIMERE observed from vertical profiles (Figure 8) is still present. Also, some discrepancies are observed especially over the ocean. Still, the correlation coefficient between both modeled fields is 0.94. We recall here that although both models use the same anthropogenic emission inventories, their configurations remain significantly different in terms of meteorology (ARPEGE/IFS), boundary conditions (MOCAGE/MOZART-IFS), chemical mechanisms (RACMOBUS/MELCHIOR2), and also discretization. Moreover, their evaluation against surface measurements and vertical profiles

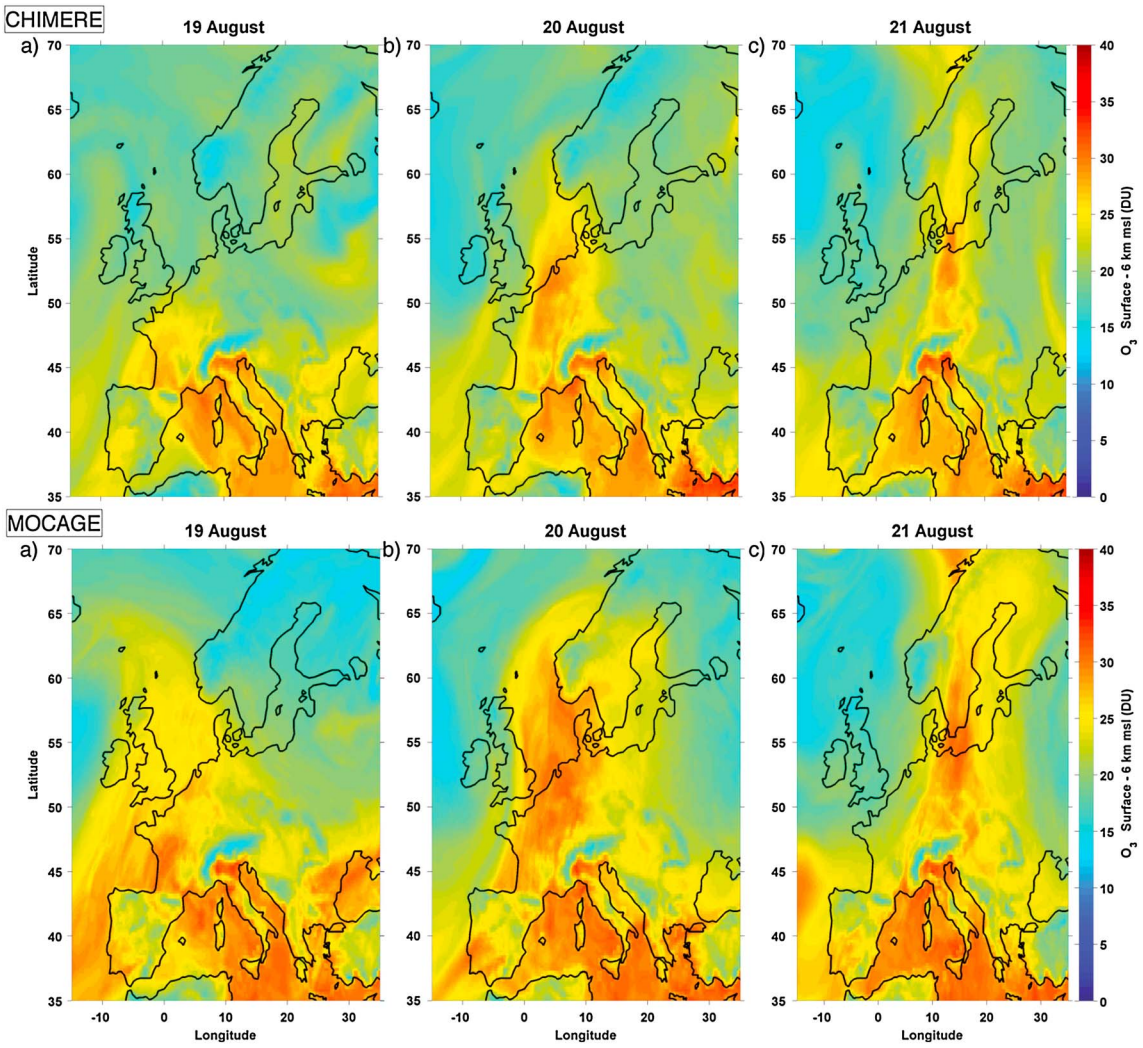

Figure 11. Surface to 6 km ozone columns (DU) simulated by CHIMERE and MOCAGE for 19–21 August 2009 at 10 A.M.

confirms their capability to well capture this pollution event (Figures 7 and 8). Also, vertical cross sections (at 45°N, 50°N, and 55°N) show that both models are quite consistent (Figures 12 and 13) in terms of simulated concentrations and of spatial and temporal ozone structures, but a greater vertical extension of the plume is generally simulated by the CHIMERE model.

This feature of the CHIMERE model is probably due to a too diffusive vertical advection scheme. We also note that both models reproduce high ozone concentrations in the upper troposphere at the western and eastern edges up to 50°N. This is consistent with high PV values given by the ECMWF (not shown).

5. Satellite Perspective

In this section, the capability of the spaceborne instruments to observe the pollution event described above is evaluated. Thus, for GOME-2, OMI, and IASI, surface to 6 km ozone columns retrieved from 19 to 21 August 2009 are displayed on Figure 14. For each instrument, observations are obtained by using the retrieval method described above (section 2). The three instruments show quite different values for surface to 6 km ozone columns during the episode. This is mainly due to differences in instrument sensitivity. Maps of degree of freedom (DOF) for the signal of the surface to 6 km columns show higher values for IASI (around 0.6) than those for GOME-2 (0.3–0.4) and OMI (0.2–0.6) (Figure 15). It should be noted that for IASI, the highest DOF values often occur over continental areas with a large thermal contrast between surface and altitude. It should be noted that TIR instruments improve their sensitivity to

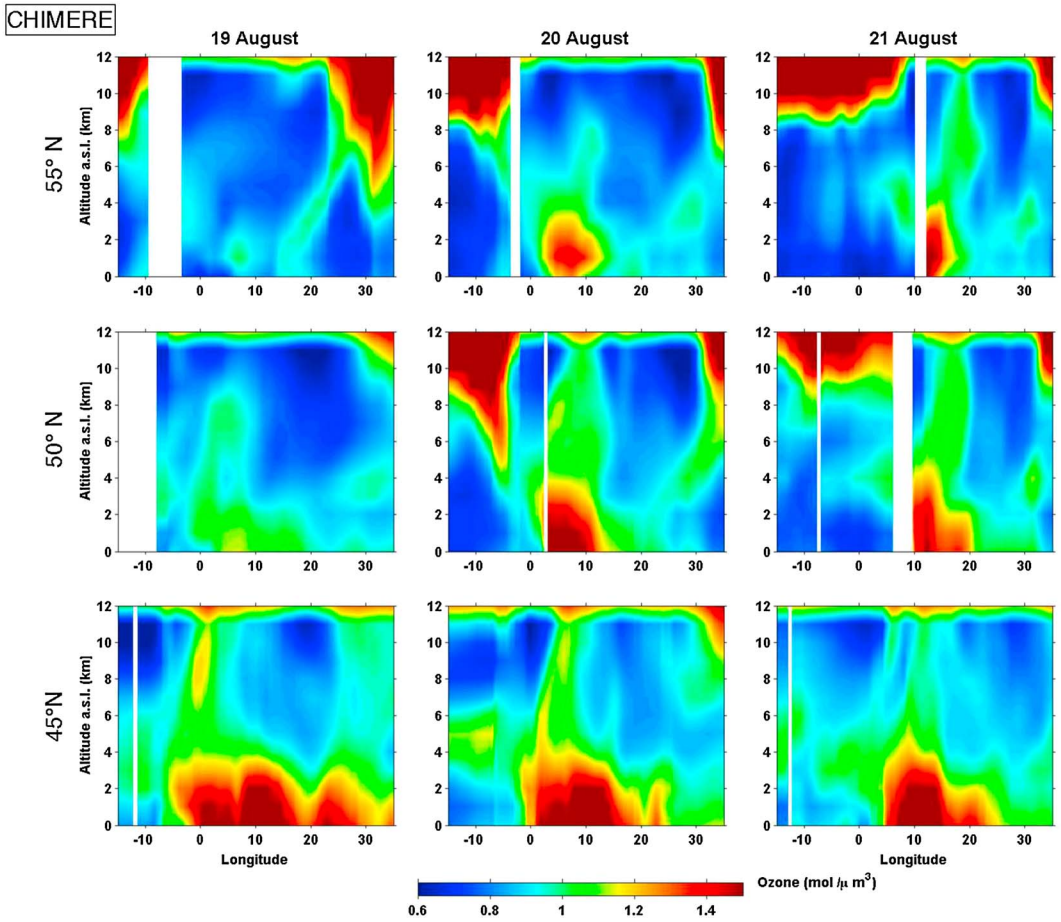

Figure 12. Vertical cross sections of ozone concentrations (mol μm^{-3}) simulated by the CHIMERE model along three latitudes (45°N, 50°N, and 55°N) and for 3 days (19–21 August 2009) at 10 A.M.

the surface in case of important thermal contrast (which is the situation during the photochemical pollution event). Enhanced DOF values appear indeed over France on 19 August and over Germany on 20 August, thus in regions of enhanced surface ozone levels. On the other hand, the highest DOFs for GOME-2 are observed for pixels with effective cloud fraction cover around 30% (above this value, pixels are not used). The higher DOF values of the IASI instrument are likely due to a weaker sensitivity to surface albedo variations and to aerosol loading; both parameters severely reduce UV instrument sensitivity in the lower troposphere [*Liu et al.*, 2010].

A qualitative comparison between satellite observations (Figure 14) and models (Figure 11) shows that the pollution plume seems only to be captured by the IASI sounder. The OMI observation is made at about 1 P.M., and model fields at 1 P.M. are rather similar to those at 3 P.M. presented on Figure 11, which thus can be used for comparison. The high ozone event characterized by the sharp gradients along the frontal area appears to be not well captured by OMI and GOME-2 observations. To be more quantitative, we have calculated the correlation coefficients between model (CHIMERE and MOCAGE) surface to 6 km ozone columns and each satellite observational field. To do this, we have selected pixels present in the rectangular area presented on Figure 14 (bottom) where the ozone plume is present. IASI gives the best correlation with both models (CHIMERE/MOCAGE) 0.74/0.74, against 0.54/0.55 for OMI and 0.38/0.47 for GOME-2 (relative RMSE also confirm these results). The lower correlation coefficients of OMI and GOME-2 are related to their lower DOF values, although model errors could also be partly responsible (if by chance, they more affect the comparison with GOME-2 and OMI than that with IASI).

Comparing the vertical distributions of ozone simulated by models (Figures 12 and 13) to IASI vertical profiles (Figure 16, left) makes evident discrepancies below 2 km height due to the low sensitivity of the instrument.

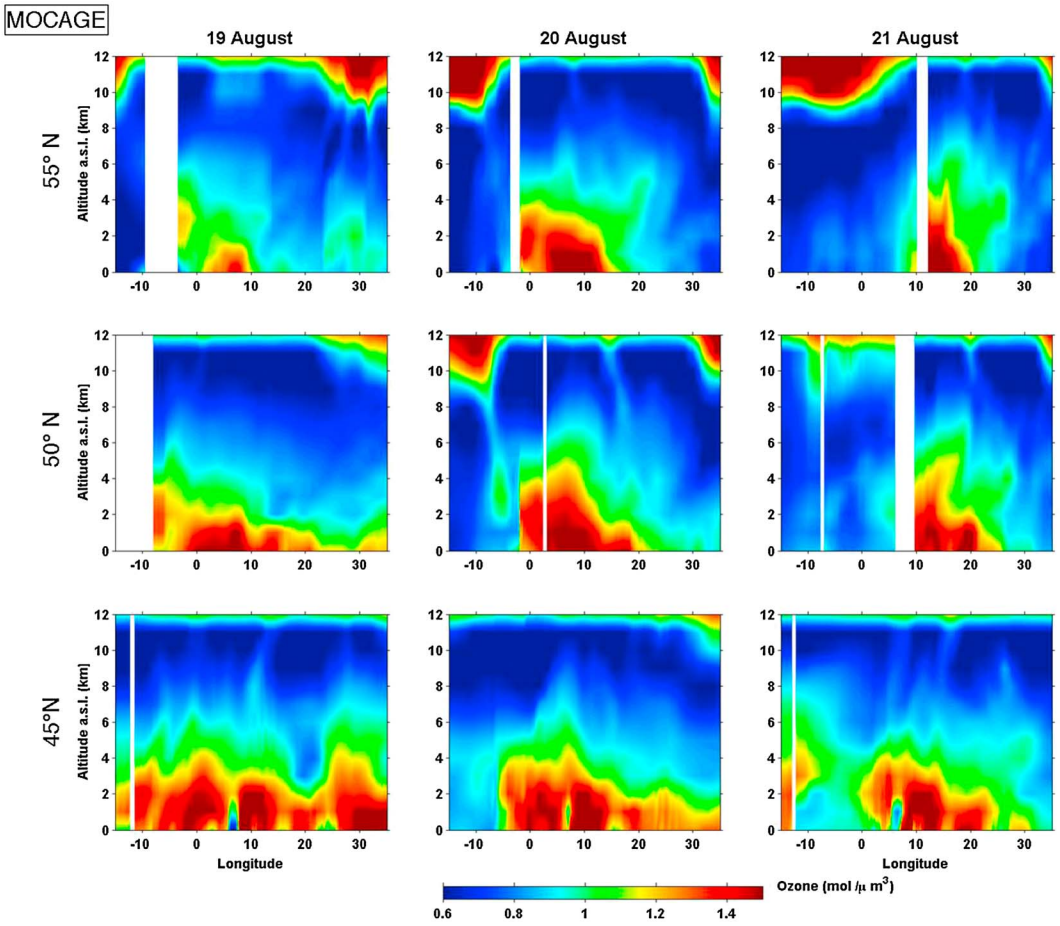

Figure 13. Vertical cross sections of ozone concentrations (mol μm^{-3}) simulated by the MOCAGE model along three latitudes (45°N, 50°N, and 55°N) and for 3 days (19–21 August 2009) at 10 A.M.

Nevertheless, on Figure 16, we clearly identify the ozone plume present at 45°N on 19 August and moving eastward and northward the next days 20 and 21 August. The dynamics of the observed plume clearly are similar to the simulated one. We also notice a negative bias between observed and simulated ozone concentrations within the plume. Vertical profiles of GOME-2 ozone are not shown since GOME-2 DOF values are really weak for this case. For OMI, Figure 16 (right) displays the ozone profiles and shows that the detection of the plume is less clear compared to IASI with lower ozone gradients and vertical resolution. If models are considered as the reference (given their good ability, as seen in section 4, to reproduce in situ measurements in that case), we can estimate what amount of tropospheric ozone is seen by the satellite by convoluting simulated fields with the averaging kernels of IASI. The convolution of CHIMERE with the averaging kernels follows the formulation proposed by *Rodgers* [2000] as described by *Coman et al.* [2012, equation 1]. These convoluted fields will indicate how the simulated field can be viewed with the "eye" of IASI. We must recall that CHIMERE, for example, shows good ability to reproduce the vertical ozone distribution during the episode (Figure 8). The result of this procedure is shown in Figure 17. CHIMERE smoothed ozone fields (i.e., simulated ozone fields, combined with IASI "a prioris" above 200 hPa, convoluted with averaging kernels of IASI) show a rather similar vertical ozone distribution than IASI observations (Figure 16). The main discrepancies occur when high ozone concentrations initially present in the upper troposphere (Figure 12) are distributed down to lower levels by applying the averaging kernels (for example, at 50°N, 10°W on 20 August and at 55°N, 10°W on 21 August). These features associated to the smoothing operation are not realistic and do not correspond to a physical feature. They only underline the weak vertical resolution of the satellite measurement. However, these features are located outside of the pollution plume area. By comparing smoothed (Figure 17) and raw (Figure 12) CHIMERE simulations, we

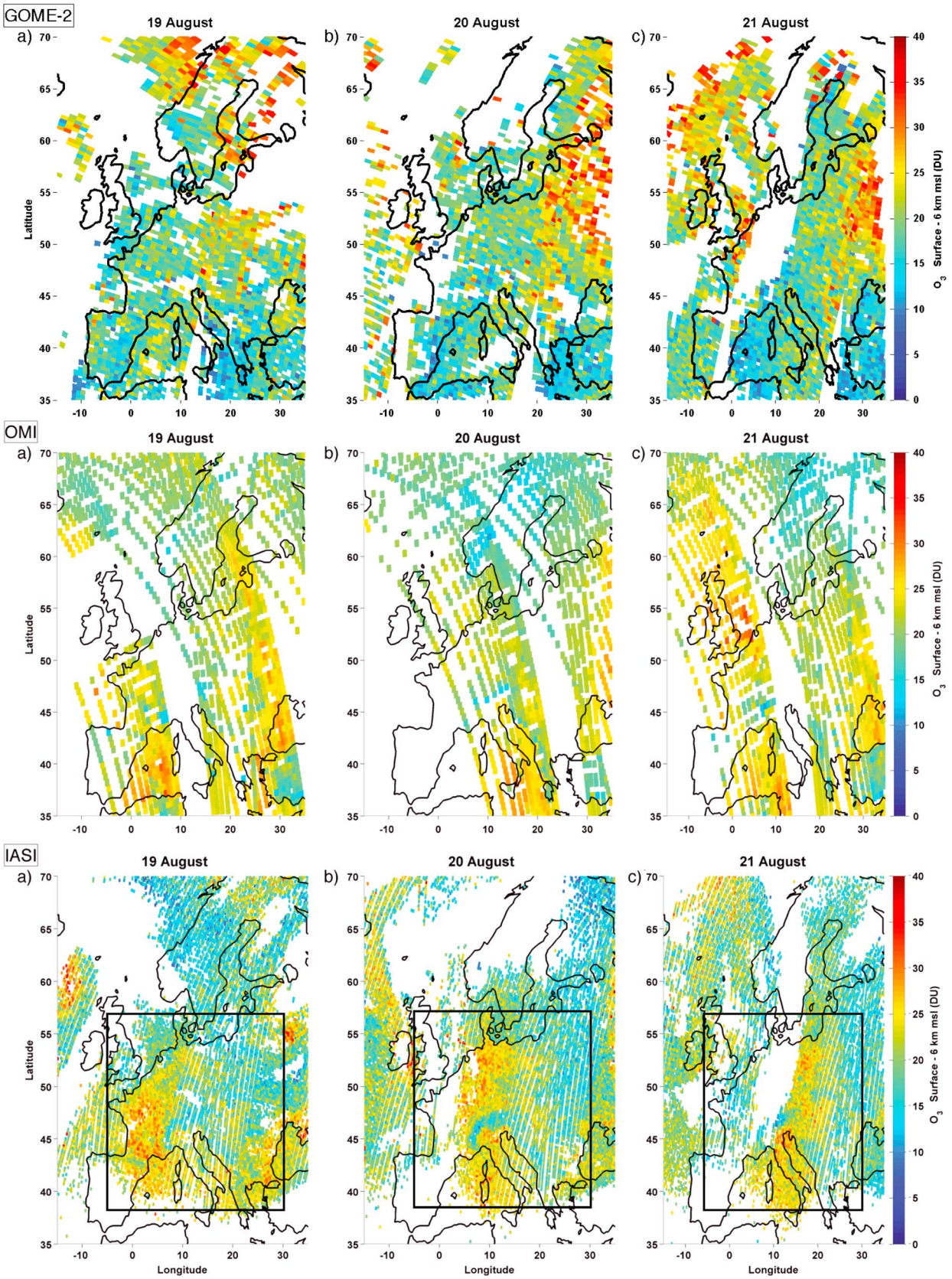

Figure 14. Surface to 6 km ozone columns retrieved by (top) GOME-2, (middle) OMI, and (bottom) IASI for 19–21 August 2009.

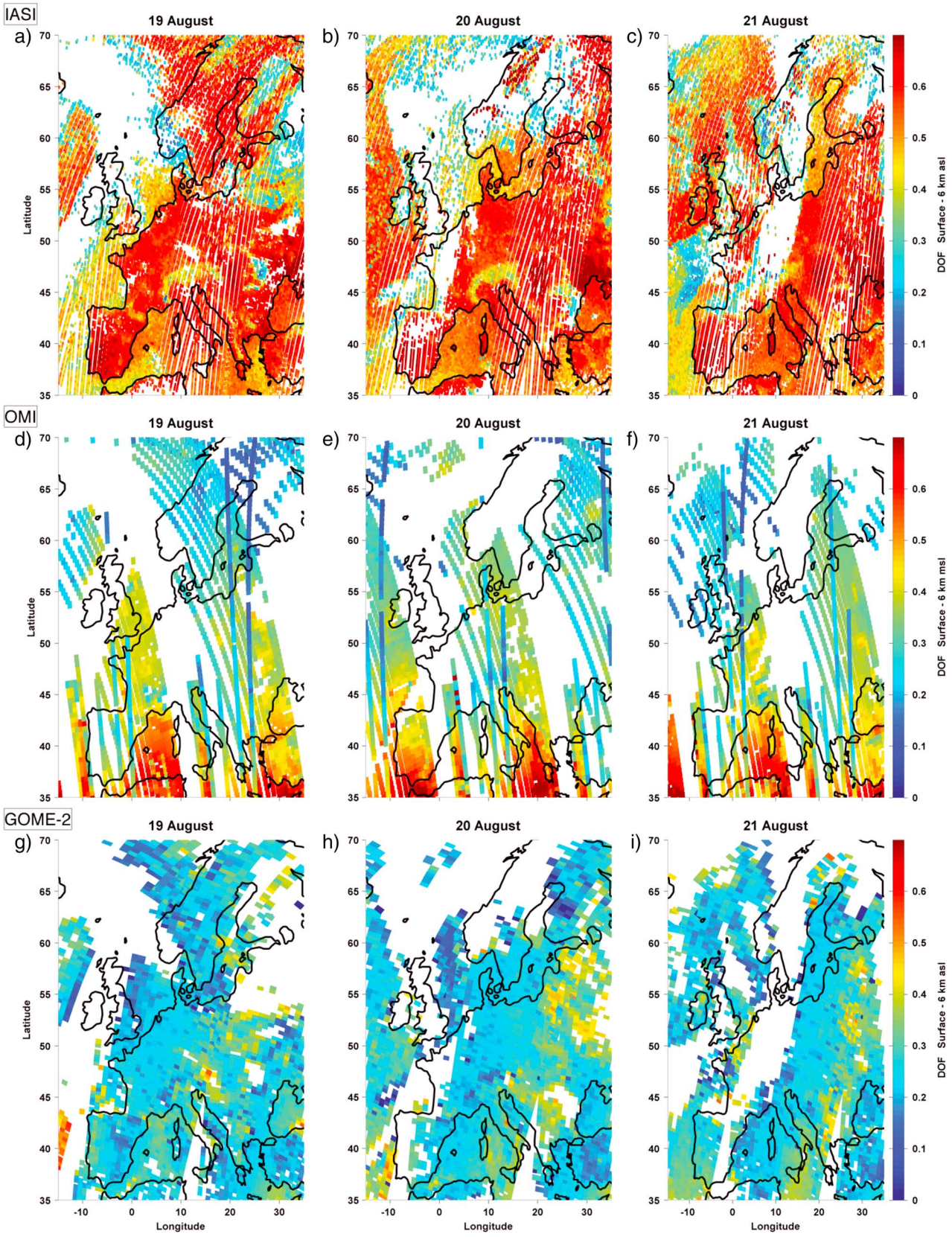

Figure 15. Degrees of freedom for signal for satellite retrievals of ozone partial column in the lower troposphere (between the surface and 6 km a.s.l.) from (a–c) IASI, (d–f) OMI, and (g–i) GOME-2, over Europe on 19–21 August.

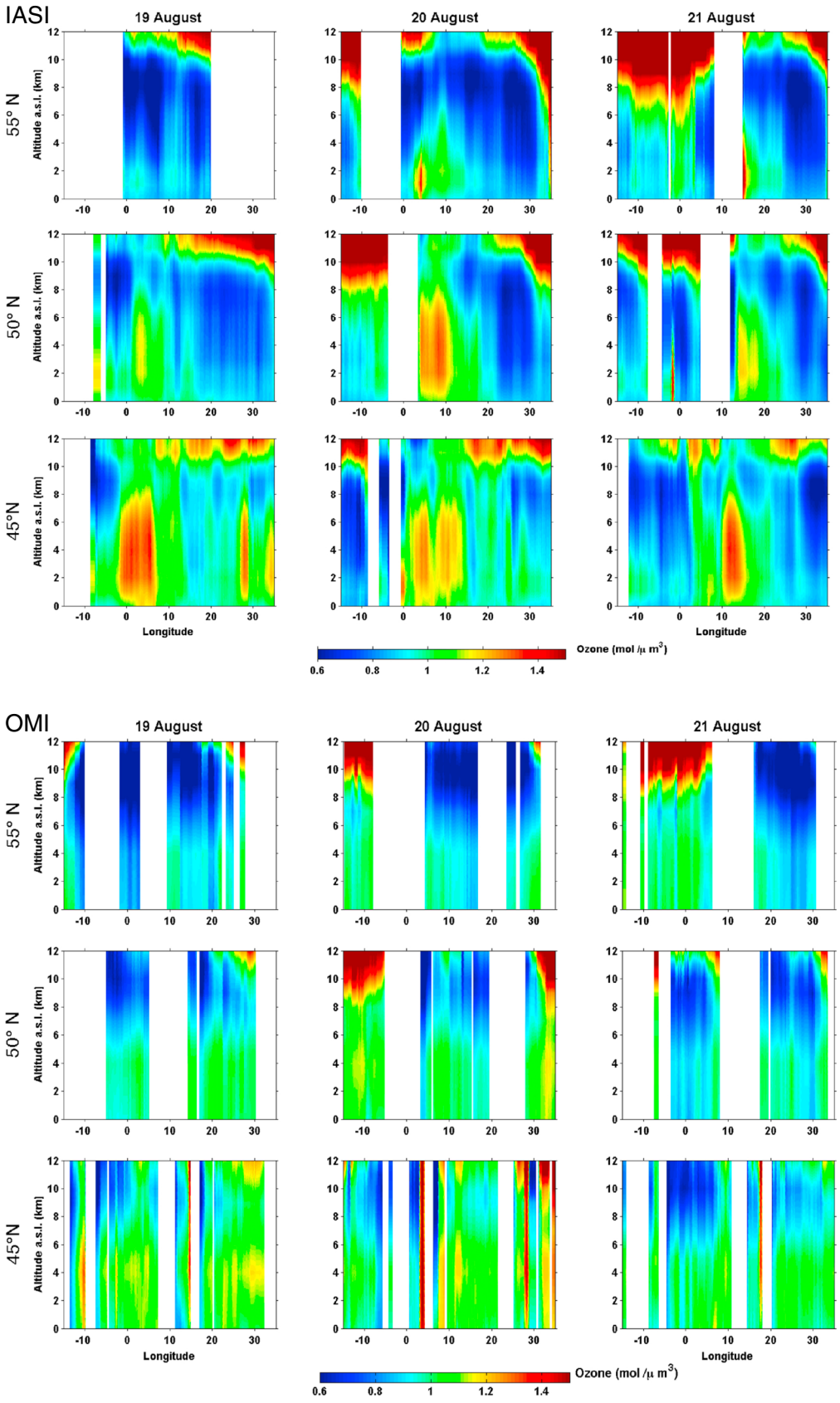

Figure 16

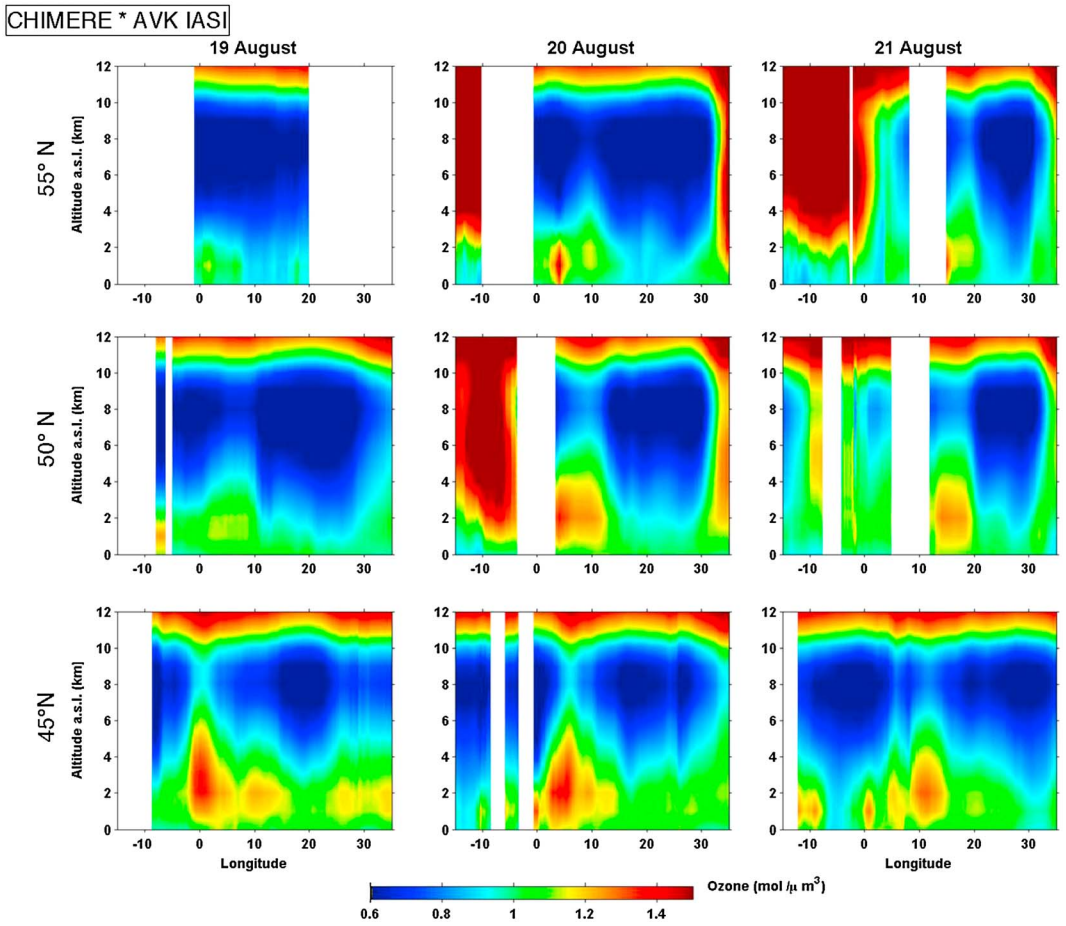

Figure 17. Vertical cross sections of ozone concentrations (mol μm^{-3}) simulated by CHIMERE and smoothed using IASI averaging kernels along three latitudes (45°N, 50°N, and 55°N) and for 3 days (19–21 2009) at 10 A.M.

notice that strong ozone concentrations simulated by CHIMERE up to 1 km height are strongly reduced in the case of smoothed fields. This confirms that IASI observations do not have an adequate sensitivity to accurately measure boundary layer ozone concentrations. The inspection of the altitude of the maximum of the averaging kernels shows values often in the range from 2 to 4 km but rarely below (not shown). Similar observations made with UV spectrometers (i.e., GOME-2 and OMI) exhibit a very different vertical structure for this episode, in line with the difficulties noted before to catch the ozone horizontal distribution. We also have used averaging kernels of GOME-2 and OMI to smooth CHIMERE vertical profiles. For GOME-2, if the spatiotemporal structure of the plume is then slightly visible, ozone concentrations remains very weak and the vertical structure not well reproduced. For OMI, it is slightly better but still far from the model output and the IASI case (not shown). These results are well in line with the analysis of the DOF values that are weaker for GOME-2 and OMI. To complete this analysis, we also have calculated (using model simulations) the fraction of the surface to 6 km ozone column present below 2 km height. It represents around 30 to 40% of the total column with a slight increase inside the plume (to 45%) for 20 August 2009 (not shown). This gives an idea of the fraction of ozone that IASI observations will probably miss.

However, from the comparisons between Figures 11 and 14, it was clearly concluded that IASI was able to capture the signature of the ozone pollution episode in the surface to 6 km partial columns, despite the lack of sensitivities to lower layers. The analysis of the vertical profiles during the episode shows that the IASI

Figure 16. Vertical cross sections of ozone concentrations (mol μm^{-3}) retrieved from (top) the IASI and (bottom) the OMI measurements along three latitudes (45°N, 50°N, and 55°N) and for 3 days (19–21 August 2009) at 10 A.M.

instrument, in reality, sees high ozone concentrations above 1 or 2 km height. It is indeed a fact that ozone concentrations present in the PBL and at higher levels (shown for 3 and 5 km in Figure 9) are correlated, which allows IASI to capture the pollution event. It is important to say that these correlations are not fortuitous; as we have shown before, they are related to the concurrent presence of an anticyclonic system at ground and of a ridge system in the free troposphere, associated to a frontal system at its western edge. These systems lead to enhanced ozone levels, either through photochemical ozone production in the boundary layer or through advection and vertical uplifting of ozone-rich air masses originating partly over the Mediterranean area. Thus, the presence of large ozone values both at ground and at higher levels is intrinsically linked. In this respect, we can positively conclude that IASI is able to "see" strong ozone pollution episodes, in the sense that it captures a system of combined enhanced ozone concentrations at ground and in the free troposphere.

From the point of view of a multiplatform observation strategy, while the observation of boundary layer ozone remains difficult, our paper shows that ozone in the lower free troposphere above the boundary layer can be detected by IASI, which is very complementary to ozone surface observations available over continental areas. Moreover, it also shows that these satellite observations can be used to characterize the transfer of boundary layer ozone to the free troposphere induced by frontal systems, which is an important process in the midlatitude free tropospheric ozone budget.

6. Conclusion and Perspectives

Current satellite ozone sounders are now able to give valuable information about tropospheric ozone concentrations. Nevertheless, their sensitivity to boundary layer ozone concentrations remains weak. We have evaluated here their capability to detect a moderate photochemical ozone episode over Europe as well as vertical transport of ozone from the PBL to the free troposphere. Indeed, these conditions with high ozone loading in the lower troposphere, low cloud cover, a potentially well-developed boundary layer, and a sharp thermal contrast are all favorable for satellite observations. We have selected a particular ozone pollution event occurring over Europe at the end of August 2009 (19–21). As shown by surface measurements, numerous exceedences of the information threshold have been observed during this period. Moreover, sharp horizontal gradients and strong lifting of surface air masses into the lower free troposphere characterize this event. This is due to a frontal pattern crossing western Europe during the 3 days of the event. This warm conveyor belt and the associated pollutant transport are well captured by two rCTMs (CHIMERE and MOCAGE). Retrievals of surface to 6 km ozone columns have been obtained from radiances measured by several instruments: GOME-2, OMI, and IASI. In this case study, only the IASI instrument (using TIR spectral domain) seems to capture the ozone field structure observed at the surface and in the lower troposphere. This is confirmed by the comparisons of satellite observations to the simulated ozone fields (from either CHIMERE or MOCAGE model). Correlations calculated between CHIMERE/MOCAGE and GOME-2, OMI, and IASI are, respectively, 0.38/0.47, 0.54/0.55, and 0.74/0.74, confirming the first qualitative finding. Moreover, vertical cross sections of satellite observations and models have confirmed the ability of the TIR sounder to detect the plume. Nevertheless, they also show that the sensitivity of satellite observations remains weak in the boundary layer and that the part of the plume that is detected is located in the free troposphere above 2 km height. Probably more case studies are needed to evaluate the ability of present satellite instruments to directly observe boundary layer ozone concentration.

We have demonstrated that the concurrent presence of an anticyclonic system at ground and of a ridge system in the free troposphere, which is a general meteorological feature, both lead to enhanced ozone levels, either through photochemical ozone production in the boundary layer or through advection and vertical uplifting of ozone-rich air masses. We thus can conclude that IASI is able capture an ozone pollution event because of this intrinsic combination of enhanced ozone concentrations at ground and in the free troposphere. In addition, this finding opens an interesting way of using the satellite to study the transfer of PBL ozone to the free troposphere. We also note that these observations are very complementary of surface observations that give a better view of PBL ozone concentrations. This clearly suggests the joint use of surface and satellite observations, for example, by data assimilation, to get improved four-dimensional ozone fields and analyses.

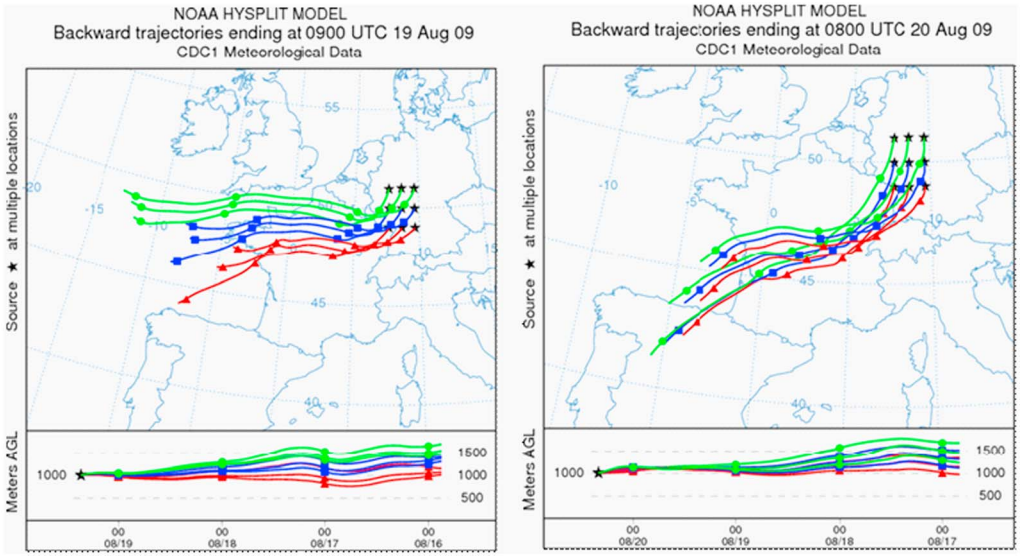

Figure A1. Frankfurt area back trajectories at 1000 km height (19 and 20 August 2009).

Considering these results, what are the perspectives for future use of satellite observations in the context of surface ozone pollution? First, it should be mentioned that existing satellite products are still evolving. The most striking example is the development of the joint retrieval of TIR and UV radiances that seems to be a promising way. Pioneering work of *Cuesta et al.* [2013] has shown that using jointly GOME-2 and IASI measurements allowed to measure ozone about 1 km below IASI sensitivity maxima keeping good accuracy. Also, *Fu et al.* [2013] show similar results using OMI and TES sounders. Indeed, the combination of both pieces of information allows, by giving a better constraint on stratospheric ozone using the UV information, to relax (increase) the TIR instrument sensitivity near the surface. However, the advantage in assimilating such a product into a CTM with respect to a combined assimilation of separate TIR and UV observations should be evaluated in a future study. Concerning future instruments, *Sellitto et al.* [2013] have shown that better sensitivity to lower tropospheric ozone and a better accuracy will be possible using the future IASI-New Generation (IASI-NG) instrument, to be launched in the 2020 timeframe as part of the EUMETSAT Polar System-Second Generation programme [*Sellitto et al.*, 2014]. At that time, following the approach of *Cuesta et al.* [2013], sensitivity to lower tropospheric ozone will be further improved by coupling IASI-NG (IASI-New

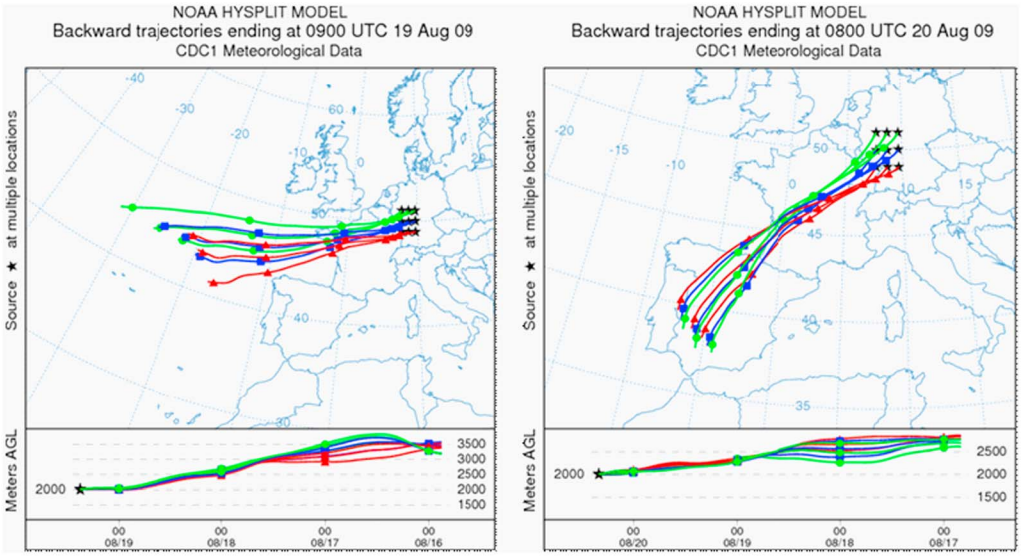

Figure A2. Frankfurt area back trajectories at 2000 km height (19 and 20 August 2009).

Generation) and the future UV/Vis sounder (onboard the same platform) measurements for joint retrievals. Also, we have to mention the possibility of having more frequent measurements given, for example, by geostationary platforms. Indeed, one of the limitations of current instruments (this is the case for IASI and GOME-2) is their revisit time. At 10 A.M., we miss ozone peaks and the thermal contrast is less pronounced than during noon and afternoon. Concerning the IRS (infrared sounder) and ultraviolet visible near-infrared instruments onboard of the geostationary MTG platform (Meteosat Troisième Génération), they could be a good opportunity to test such high temporal sampling even if these instruments will have limited accuracy (especially IRS compared to IASI or IASI-NG). Projects for future geostationary missions dedicated to atmospheric composition are now numerous [*Fishman et al.*, 2012; *Peuch et al.*, 2010; *Chance et al.*, 2013]. Especially, the idea is to have high-accuracy instruments using multispectral coupling onboard of such platforms or constellation of platforms [*Bowman*, 2013]. These future platforms will probably allow to greatly improve future air quality monitoring from space and forecasting systems assimilating their observations.

Appendix A

Additional back trajectories calculated with the HYSPLIT model are provided here to complement the analysis of the air mass trajectories arriving at Frankfurt and to explain the vertical profile of ozone observed at Frankfurt airport. Back trajectories arriving at Frankfurt and at 1 km and 2 km altitude on 19–20 August 2009 are provided (Figures A1 and A2).

Acknowledgments

The research leading to these results has received funding from the European Community's Seventh Framework Programme (FP7 THEME [SPA.2011.1.5-02]) under grant agreement n.283576, i.e., the MACC-II project. This study was supported by the project "IASI-TOSCA" (Terre, Océan, Surfaces continentals, Atmosphère) financed by CNES. This work was granted access to the HPC resources of CCRT under the allocation 2013-6695 made by GENCI (Grand Equipement National de Calcul Intensif). IASI has been developed and built under the responsibility of the Centre National d'Etudes Spatiales (CNES, France). It is flown aboard the MetOp satellites as part of the EUMETSAT Polar System. We acknowledge the support by the data centers ETHER (http://www.pole-ether.fr/) and NOAA CLASS (http://www.class.ncdc.noaa.gov) for providing respectively L1 IASI and GOME-2 data sets, which are originally supplied by EUMETSAT through the Eumetcast system distribution (http://www.eumetsat.int). The Dutch-Finnish OMI instrument is part of the NASA EOS Aura satellite payload. The OMI Project is managed by NIVR and KNMI in the Netherlands. We acknowledge the OMI International Science Team for providing satellite data used in this study. X. Liu is funded by NASA and the Smithsonian Institution. This work is also part of the ADOMOCA-II project funded by the French LEFE program (CHAT/ASSIM). The authors gratefully acknowledge the NOAA Air Resources Laboratory (ARL) for the provision of the HYSPLIT transport and dispersion model and/or READY website (http://www.ready.noaa.gov) used in this publication. RMIB, MeteoSwiss, DWD-MOL, PIMWM, AEMET & KNMI. World Ozone and Ultraviolet Radiation Data Centre (WOUDC) [Data]. Retrieved in 2013, from http://www.woudc.org. The authors acknowledge the strong support of the European Commission, Airbus, and airlines—Lufthansa, Air France, Austrian, and former Sabena—to the MOZAIC program.

References

Agustí-Panareda, A., S. Gray, and J. Methven (2005), Numerical modeling study of boundary-layer ventilation by a cold front over Europe, *J. Geophys. Res.*, *110*, D18304, doi:10.1029/2004JD005555.

Agustí-Panareda, A., S. L. Gray, and S. E. Belcher (2009), On the dependence of boundary layer ventilation on frontal type, *J. Geophys. Res.*, *114*, D05305, doi:10.1029/2008JD010694.

Barré, J., V.-H. Peuch, J.-L. Attié, L. El Amraoui, W. A. Lahoz, B. Josse, M. Claeyman, and P. Nédélec (2012), Stratosphere-troposphere ozone exchange from high resolution MLS ozone analyses, *Atmos. Chem. Phys.*, *12*, 6129–6144.

Barré, J., et al. (2013), Combined data assimilation of ozone tropospheric columns and stratospheric profiles in a high-resolution CTM, *Q. J. R. Meteorol. Soc.*, *140*, 966–981, doi:10.1002/qj.2176.

Bechtold, P., E. Bazile, F. Guichard, P. Mascart, and E. Richard (2001), A mass flux convection scheme for mesoscale and global models, *Q. J. R. Meteorol. Soc.*, *126*, 865–889.

Bethan, S., G. Vaughan, C. Gerbig, A. Volz-Thomas, H. Richer, and D. A. Tiddeman (1998), Chemical air mass differences near fronts, *J. Geophys. Res.*, *103*, 13,413–13,434, doi:10.1029/98JD00535.

Blond, N., and R. Vautard (2004), Three-dimensional ozone analyses and their use for short-term ozone forecasts, *J. Geophys. Res.*, *109*, D17303, doi:10.1029/2004JD004515.

Bousserez, N., J.-L. Attié, V.-H. Peuch, M. Michou, G. Pfister, D. Edwards, M. Avery, G. Sachse, E. Browell, and E. Ferrare (2007), Evaluation of MOCAGE chemistry and transport model during the ICARTT/ITOP experiment, *J. Geophys. Res.*, *112*, D10S42, doi:10.1029/2006JD007595.

Bovensmann, H., J. P. Burrows, M. Buchwitz, J. Frerick, S. Noël, V. V. Rozanov, K. V. Chance, and A. H. P. Goede (1999), SCHIAMACHY: Mission objectives and measurement modes, *J. Atmos. Sci.*, *56*, 127–150.

Bowman, K. W. (2013), Toward the next generation of air quality monitoring: Ozone, *Atmos. Environ.*, *80*, 571–583.

Boynard, A., C. Clerbaux, P.-F. Coheur, D. Hurtmans, S. Turquety, M. George, J. Hadji-Lazaro, C. Keim, and J. Meyer-Arnek (2009), Measurements of total and tropospheric ozone from IASI: Comparison with correlative satellite, ground-based and ozonesonde observations, *Atmos. Chem. Phys.*, *9*, 6255–6271, doi:10.5194/acp-9-6255-2009.

Braak, R. (2010), Bug fix for GDPS measurement noise calculation algorithm, *Tech. Note TN-OMIE-KNMI-935*, KNMI.

Burrows, J. P., et al. (1999), The Global Ozone Monitoring Experiment (GOME): Mission concept and first scientific results, *J. Atmos. Sci.*, *56*, 151–175.

Cai, Z., Y. Liu, X. Liu, K. Chance, C. R. Nowlan, R. Lang, R. Munro, and R. Suleiman (2012), Characterization and correction of Global Ozone Monitoring Experiment 2 ultraviolet measurements and application to ozone profile retrievals, *J. Geophys. Res.*, *117*, D07305, doi:10.1029/2011JD017096.

Chance, K., X. Liu, R. M. Suleiman, D. E. Flittner, J. Al-Saadi, and S. J. Janz (2013), Tropospheric emissions: Monitoring of pollution (TEMPO), *Proc. SPIE* 8866, Earth Observing Systems XVIII, 88660D, doi:10.1117/12.2024479.

Clarisse, L., C. Clerbaux, F. Dentener, D. Hurtmans, and P.-F. Coheur (2009), Global ammonia distribution derived from infrared satellite observations, *Nat. Geosci.*, *2*, 479–483.

Clerbaux, C., et al. (2009), Monitoring of atmospheric composition using the thermal infrared IASI/MetOp sounder, *Atmos. Chem. Phys.*, *9*, 6041–6054.

Colella, P., and P. R. Woodward (1984), The piecewise parabolic method (PPM) for gas-dynamical simulations, *J. Comput. Phys.*, *11*, 38–39.

Coman, C., G. Foret, M. Beekmann, M. Eremenko, G. Dufour, B. Gaubert, A. Ung, C. Schmechtig, J.-M. Flaud, and G. Bergametti (2012), Assimilation of IASI partial tropospheric columns with an Ensemble Kalman Filter over Europe, *Atmos. Chem. Phys.*, *12*, 2513–2532.

Courtier, P., C. Freydier, J. F. Geleyn, F. Rabier, and M. Rochas (1991), The ARPEGE project at Météo France, in *Atmospheric Models*, vol. 2, pp. 193–231, Workshop on Numerical Methods, Reading, U. K.

Crutzen, P. J., M. G. Lawrence, and U. Pöschl (1999), On the background photochemistry of tropospheric ozone, *Tellus B*, *51*(1), 123–146.

Cuesta, J., et al. (2013), Satellite observation of lowermost tropospheric ozone by multispectral synergism of IASI thermal infrared and GOME-2 ultraviolet measurements, *Atmos. Chem. Phys.*, *13*, 9675–9693.

Dentener, F., D. Stevenson, J. Cofala, R. Mechler, M. Amann, P. Bergamaschi, F. Raes, and R. Derwent (2005), The impact of air pollutant and methane emission controls on tropospheric ozone and radiative forcing: CTM calculations for the period 1990–2030, *Atmos. Chem. Phys.*, *5*, 1731–1755, doi:10.5194/acp-5-731-2005.

Dufour, G., M. Eremenko, J. Orphal, and J.-M. Flaud (2010), IASI observations of seasonal and day-to-day variations of tropospheric ozone over three highly populated areas of China: Beijing, Shanghai, and Hong Kong, *Atmos. Chem. Phys.*, *10*, 3787–3801.

Dufour, G., M. Eremenko, A. Griesfeller, B. Barret, E. LeFlochmoën, C. Clerbaux, J. Hadji-Lazaro, P.-F. Coheur, and D. Hurtmans (2012), Validation of three different scientific ozone products retrieved from IASI spectra using ozonesondes, *Atmos. Meas. Tech.*, *5*, 611–630.

Elbern, H., and H. Schmidt (2001), Ozone episode analysis by four-dimensional variational chemistry data assimilation, *J. Geophys. Res.*, *106*, 3569–3590, doi:10.1029/2000JD900448.

Eremenko, M., G. Dufour, G. Foret, C. Keim, J. Orphal, M. Beekmann, G. Bergametti, and J.-M. Flaud (2008), Tropospheric ozone distributions over Europe during the heat wave in July 2007 observed from infrared nadir spectra recorded by IASI, *Geophys. Res. Lett.*, *35*, L18805, doi:10.1029/2008GL034803.

European Environmental Agency technical report (2010), Air pollution by ozone across Europe during summer 2009, N°2/2010, ISSN 1725-2237.

European Environmental Agency technical report (2013a), Air pollution by ozone across Europe during summer 2012, N°3/2013, ISSN 1725-2237.

European Environmental Agency report (2013b), Air quality in Europe—2013 report, No 9/2013, ISSN 1725-9177.

European Organisation for the Exploitation of Meteorological Satellites (2006), GOME-2 Level 1 product generation specification, EPS.SYS. SPE.990011, Darmstadt, Germany.

Fiore, A. M., et al. (2009), Multimodel estimates of intercontinental source-receptor relationships for ozone pollution, *J. Geophys. Res.*, *114*, D04301, doi:10.1029/2008JD010816.

Fishman, J., et al. (2012), The United States' next generation of atmospheric composition and coastal ecosystem measurements: NASA's Geostationary Coastal and Air Pollution Events (Geo-Cape) Mission, *Bull. Am. Meteorol. Soc.*, *93*, 1547–1566, doi:10.1175/BAMS-D-11-00201.1.

Foret, G., L. Hamaoui, C. Schmechtig, M. Eremenko, C. Keim, G. Dufour, A. Boynard, A. Coman, A. Ung, and M. Beekmann (2009), Evaluating the potential of IASI ozone observations to constrain simulated surface ozone concentrations, *Atmos. Chem. Phys.*, *9*, 8479–8491.

Forster, P., et al. (2007), Changes in atmospheric constituents and in radiative forcing, in *Climate Change 2007: The Physical Science Basis. Contribution of Working Group I to the Fourth Assessment Report of the Intergovernmental Panel on Climate Change*, edited by S. Solomon et al., 996 pp., Cambridge Univ. Press, Cambridge, U. K., and New York.

Fu, D., J. R. Worden, X. Liu, S. S. Kulawik, K. W. Bowman, and V. Natraj (2013), Characterization of ozone profiles derived from Aura TES and OMI radiances, *Atmos. Chem. Phys.*, *13*, 3445–3462.

Gaubert, B., A. Coman, G. Foret, F. Meleux, A. Ung, L. Rouil, A. Ionescu, Y. Candau, and M. Beekmann (2014), Regional scale ozone data assimilation using an ensemble Kalman filter and the CHIMERE chemical transport model, *Geosci. Model Dev.*, *7*, 283–302.

George, M., et al. (2009), Carbon monoxide distributions from the IASI/METOP mission: Evaluation with other space-borne remote sensors, *Atmos. Chem. Phys.*, *9*, 8317–8330, doi:10.5194/acp-9-8317-2009.

Guenther, A., T. Karl, P. Harley, C. Wiedinmyer, P. I. Palmer, and C. Geron (2006), Estimates of global terrestrial isoprene emissions using MEGAN (Model of Emissions of Gases and Aerosols from Nature), *Atmos. Chem. Phys.*, *6*, 3181–3210, doi:10.5194/acp-6-3181-2006.

Guenther, A. B., et al. (1995), A global model of natural volatile compound emissions, *J. Geophys. Res.*, *100*, 8873–8892, doi:10.1029/94JD02950.

Hanea, G. R., G. J. M. Velders, and A. Heemink (2004), Data assimilation of ground-level ozone in Europe with a Kalman filter and chemistry transport model, *J. Geophys. Res.*, *109*, D10302, doi:10.1029/2003JD004283.

Hayes, F., G. Mills, H. Harmens, and D. Norris (2007), *Evidence of Widespread Ozone Damage to Vegetation in Europe (1990–2006)*, ICP Vegetation Programme Coordination Centre, CEH, Bangor, U. K.

Huang, H., et al. (2013), Impacts of transported background pollutants on summertime western US air quality: Model evaluation, sensitivity analysis and data assimilation, *Atmos. Chem. Phys.*, *13*, 359–391.

Jaumouillé, E., S. Massart, A. Piacentini, D. Cariolle, and V.-H. Peuch (2012), Impact of a time-dependent background error covariance matrix on air quality analysis, *Geosci. Model Dev.*, *5*, 1075–1090.

Josse, B., P. Simon, and V.-H. Peuch (2004), Rn-222 global simulations with the multiscale CTM MOCAGE, *Tellus B*, *56*, 339–356.

Kar, J., J. Fishman, J. K. Creilson, A. Richter, J. Ziemke, and S. Chandra (2010), Are there urban signatures in the tropospheric ozone column products derived from satellite measurements?, *Atmos. Chem. Phys.*, *10*, 5213–5222.

Keim, C., et al. (2009), Tropospheric ozone from IASI: Comparison of different inversion algorithms and validation with ozone sondes in the northern middle latitudes, *Atmos. Chem. Phys.*, *9*, 9329–9347.

Kim, P. S., D. J. Jacob, X. Liu, J. X. Warner, K. Yang, K. Chance, V. Thouret, and P. Nedelec (2013), Global ozone–CO correlations from OMI and AIRS: Constraints on tropospheric ozone sources, *Atmos. Chem. Phys.*, *13*, 9321–9335, doi:10.5194/acp-13-9321-2013.

Kowol-Santen, J., M. Beekman, S. Schmitgen, and K. Dewey (2001), Tracer analysis of transport from the boundary layer to the free troposphere, *Geophys. Res. Lett.*, *28*, 2907–2910, doi:10.1029/2001GL012908.

Kukkonen, J., et al. (2012), A review of operational, regional-scale, chemical weather forecasting models in Europe, *Atmos. Chem. Phys.*, *12*(1), 1–87.

Lefèvre, F., G. P. Brasseur, I. Folkins, A. K. Smith, and P. Simon (1994), Chemistry of the 1991–1992 stratospheric winter: Three-dimensional model simulations, *J. Geophys. Res.*, *99*, 8183–8195, doi:10.1029/93JD03476.

Levelt, P. F., G. H. J. van den Ord, M. R. Dobber, A. Mlkki, H. Visser, J. de Vries, P. Stammes, J. O. V. Lundell, and H. Saari (2006), The Ozone Monitoring Instrument, *IEEE Trans. Geosci. Remote Sens.*, *44*, 1093–1101.

Liu, J. J., D. B. A. Jones, J. R. Worden, D. Noone, M. Parrington, and J. Kar (2009), Analysis of the summertime buildup of tropospheric ozone abundances over the Middle East and North Africa as observed by the Tropospheric Emission Spectrometer instrument, *J. Geophys. Res.*, *114*, D05304, doi:10.1029/2008JD010993.

Liu, X., P. K. Bhartia, K. Chance, R. J. D. Spurr, and T. P. Kurosu (2010), Ozone profile retrievals from the Ozone Monitoring Instrument, *Atmos. Chem. Phys.*, *10*, 2521–2537.

Louis, J. F. (1979), A parametric model of vertical eddy fluxes in the atmosphere, *Boundary Layer Meteorol.*, *17*, 197–202.

Marenco, A., et al. (1998), Measurement of ozone and water vapour by Airbus in-service aircraft: The MOZAIC airborne program, an overview, *J. Geophys. Res.*, *103*, 25,631–25,642, doi:10.1029/98JD00977.

Menut, L., et al. (2013), CHIMERE 2013: A model for regional atmospheric composition modeling, *Geosci. Model Dev.*, *6*, 981–1028.

Michou, M., and V.-H. Peuch (2002), Surface exchanges in the multi-scale chemistry and transport model MOCAGE, *Water Sci. Rev.*, *15*, 173–203.

Parrington, M., D. B. A. Jones, K. W. Bowman, L. W. Horowitz, A. M. Thompson, D. W. Tarasick, and J. C. Witte (2008), Estimating the summertime tropospheric ozone distribution over North America through assimilation of observations from the Tropospheric Emission Spectrometer, *J. Geophys. Res.*, *113*, D18307, doi:10.1029/2007JD009341.

Parrington, M., D. B. A. Jones, K. W. Bowman, A. M. Thompson, D. W. Tarasick, J. Merrill, S. J. Oltmans, T. Leblanc, J. C. Witte, and D. B. Millet (2009), Impact of the assimilation of ozone from the Tropospheric Emission Spectrometer on surface ozone across North America, *Geosphys. Res. Lett.*, *36*, L04802, doi:10.1029/2008GL036935.

Peuch, V.-H., et al. (2010), MAGEAQ—Monitoring the Atmosphere from Geostationary orbit for European Air Quality: A candidate for Earth Explorer Opportunity Mission EE-8, *Tech. Rep.*

Rao, S. T., S. Galmarini, and K. Puckett (2011), Air Quality Model Evaluation International Initiative (AQMEII), *Bull. Am. Meteorol. Soc.*, *92*, 23–30, doi:10.1175/2010BAMS3069.1.

Richards, N. A. D., S. R. Arnold, M. P. Chipperfield, G. Miles, A. Rap, R. Siddans, S. A. Monks, and M. J. Hollaway (2013), The Mediterranean summertime ozone maximum: Global emission sensitivities and radiative impacts, *Atmos. Chem. Phys.*, *13*, 2331–2345.

Rodgers, C. D. (2000), *Inverse Methods for Atmospheric Sounding: Theory and Practice, World Scientific, Ser. Atmos. Ocean. Planet. Phys.*, vol. 2, 200 pp., Hackensack, N. J.

Rolph, G. D. (2013), Real-time Environmental Applications and Display sYstem (READY) Website [Available at http://www.ready.noaa.gov], NOAA Air Resources Laboratory, College Park, Md.

Schmidt, H., C. Derognat, R. Vautard, and M. Beekmann (2001), A comparison of simulated and observed ozone mixing ratios for the summer of 1998 in western Europe, *Atmos. Environ.*, *35*, 6277–6297.

Sellitto, P., B. R. Bojkov, X. Liu, K. Chance, and F. Del Frate (2011), Tropospheric ozone column retrieval at northern mid-latitudes from the Ozone Monitoring Instrument by means of a neural network algorithm, *Atmos. Meas. Tech.*, *4*, 2375–2388.

Sellitto, P., G. Dufour, M. Eremenko, J. Cuesta, P. Dauphin, G. Forêt, B. Gaubert, M. Beekmann, V.-H. Peuch, and J.-M. Flaud (2013), Analysis of the potential of one possible instrumental configuration of the next generation of IASI instruments to monitor lower tropospheric ozone, *Atmos. Meas. Tech.*, *6*, 621–635.

Sellitto, P., G. Dufour, M. Eremenko, J. Cuesta, G. Forêt, B. Gaubert, M. Beekmann, V.-H. Peuch, and J.-M. Flaud (2014), Monitoring the lowermost tropospheric ozone with thermal infrared observations from a geostationary platform: Performance analyses for a future dedicated instrument, *Atmos. Meas. Tech.*, *7*, 391–407.

Sinclair, V. A., S. L. Gray, and S. E. Belcher (2008), Boundary-layer ventilation by baroclinic life cycles, *Q. J. R. Meteorol. Soc.*, *134*, 1409–1424.

Sitch, S., P. M. Cox, W. J. Collins, and C. Huntingford (2007), Indirect radiative forcing of climate change through ozone effects on the land-carbon sink, *Nature*, *448*, 791–794.

Solazzo, E., et al. (2012), Model evaluation and ensemble modelling of surface-level ozone in Europe and North America in the context of AQMEII, *Atmos. Environ.*, *53*, 60–74.

Stockwell, W. R., F. Kirchner, M. Khun, and S. Seefeld (1997), A new mechanism for regional atmospheric chemistry modelling, *J. Geophys. Res.*, *102*, 25,847–25,879, doi:10.1029/97JD00849.

Tiedtke, M. (1989), A comprehensive mass flux scheme for cumulus parameterization in large-scale models, *Mon. Weather Rev.*, *117*, 1779–1800.

Troen, I., and L. Mahrt (1986), A simple model of the atmospheric boundary layer: Sensitivity to surface evaporation, *Boundary Layer Meteorol.*, *37*, 129–148.

Van Leer, B. (1979), Towards the ultimate conservative difference scheme. A second-order sequel to Godunov's method, *J. Comput. Phys.*, *32*, 101–136.

Visschedijk, A. J. H., P. Y. J. Zandveld, and H. A. C. A. Denier van der Gon (2007), High resolution gridded European database for the EU Integrate Project GEMS, TNO-report 2007-A-R0233/B.

Wang, L., M. J. Newchurch, A. Biazar, X. Liu, S. Kuang, M. Khan, and K. Chance (2011), Evaluating AURA/OMI ozone profiles using ozonesonde data and EPA surface measurements for August 2006, *Atmos. Environ.*, *45*, 5523–5530.

Wesely, M. L. (1989), Parameterizations of surface resistance to gaseous dry deposition in regional-scale numerical models, *Atmos. Environ.*, *23*, 1293–1304.

Williamson, D. L., and P. J. Rash (1989), Two-dimensional semi-Lagrangian transport with shape-preserving interpolation, *Mon. Weather Rev.*, *117*, 102–129.

Worden, H. M., et al. (2007), Comparisons of Tropospheric Emission Spectrometer (TES) ozone profiles to ozonesondes: Methods and initial results, *J. Geophys. Res.*, *112*, D03309, doi:10.1029/2006JD007258.

Worden, J., et al. (2009), Observed vertical distribution of tropospheric ozone during the Asian summertime monsoon, *J. Geophys. Res.*, *114*, D13304, doi:10.1029/2008JD010560.

World Health Organization (2013), Health aspects of air pollution with particulate matter, ozone and nitrogen dioxide, Report on a WHO Working Group, Regional Office for Europe; Bonn, Germany 13–15 January 2003. EUR/03/5042688.

Wu, L., V. Mallet, M. Bocquet, and B. Sportisse (2008), A comparison study of data assimilation algorithms for ozone forecast, *J. Geophys. Res.*, *113*, D20310, doi:10.1029/2008JD009991.

Zhang, L., J. R. Brook, and R. Vet (2003), A revised parameterization for gaseous dry deposition in air-quality models, *Atmos. Chem. Phys.*, *3*, 2067–2082, doi:10.5194/acp-3-2067-2003.

Zyryanov, D., et al. (2012), 3-D evaluation of tropospheric ozone simulations by an ensemble of regional Chemistry Transport Model, *Atmos. Chem. Phys.*, *12*, 3219–3240.